MECHANICAL PROPERTY MEASUREMENT BY INDENTATION TECHNIQUES

A Thesis

by

BALASUBRAMANIAN JANAKIRAMAN

Submitted to the Office of Graduate Studies of
Texas A&M University
in partial fulfillment of the requirements for the degree of

MASTER OF SCIENCE

December 2004

Major Subject: Mechanical Engineering

MECHANICAL PROPERTY MEASUREMENT BY INDENTATION TECHNIQUES

A Thesis

by

BALASUBRAMANIAN JANAKIRAMAN

Submitted to the Office of Graduate Studies of
Texas A&M University
in partial fulfillment of the requirements for the degree of

MASTER OF SCIENCE

Approved as to style and content by:

Jyhwen Wang (Co-Chair of Committee)	Richard Alexander (Co-Chair of Committee)
Karl Hartwig (Member)	Dennis O'Neal (Head of Department)

December 2004

Major Subject: Mechanical Engineering

ABSTRACT

Mechanical Property Measurement by Indentation Techniques.

(December 2004)

Balasubramanian Janakiraman, B. Engg., Madurai Kamaraj University, India

Co-Chairs of Advisory Committee: Dr. Jyhwen Wang
Dr. Richard Alexander

The mechanical properties of materials are usually evaluated by performing a tensile or hardness test on the sample. Tensile tests are often time consuming, destructive and need specially prepared specimens. On the other hand, there is no direct theoretical correlation between the hardness number and the mechanical properties of a material although phenomenological relationships do exist. The advantages of indentation techniques are that they are non-destructive, quick, and can be applied to small material samples and localized in fashion. Mechanical properties are typically determined from spherical indentation load-depth curves. This process is again a time consuming one and not suitable for situations where a quick assessment is required such as in the sheet metal rolling industry.

In the present study, a novel method of measuring mechanical properties of the material by multiple spherical indentations is developed. A series of indentations are made on the substrate with a spherical indenter with different loads. The diameter of the indentation is related to the load applied to determine the mechanical properties of the material, namely the yield strength and the work hardening parameters. To determine the diameter of the indentation quickly, a fiber optic sensing technique is developed. An incident light beam

from a semiconductor laser is coupled back into an optical fiber upon reflection from the metal surface. By measuring the diffused light power reflected from the metal surface, the diameter of the indentation is measured.

The spherical indentation technique is difficult for real time mechanical property measurement of sheet metal in a processing line. Problems arise as the strip is traveling at 2,000 to 4,000 ft/min (10,000 to 20,000 mm/sec) in the processing line. As a first step in developing a process that could be implemented in a real time processing line, a preliminary study has been conducted for the prediction of yield strength by laser shock processing.

Dedicated to my mother Padma and father Janakiraman who have worked hard throughout their lives for my education and gave me the opportunity to come to the United States of America for higher studies.

ACKNOWLEDGMENTS

I would like to take this opportunity to express my deep gratitude to Dr. Jyhwen Wang for giving me the opportunity to work on this research project and his guidance to its completion. Whenever I had problems in my research, he was there to patiently explain things to me. He constantly inspired and motivated me to achieve my academic goals. I would like to thank Dr. Chin Su for his guidance in the development of fiber optics sensing technique.

It gives me immense pleasure in expressing my heartfelt gratitude to Dr. Richard Alexander for all the cooperation he has rendered in the successful completion of this work. I would also like to thank Dr. Karl Hartwig for serving on my thesis committee. I would also like to thank ALCOA Technical Center for their financial support for the development of the fiber optic sensing technique.

TABLE OF CONTENTS

Page

LIST OF FIGURES

FIGURE Page

LIST OF TABLES

1. INTRODUCTION

Mechanical properties are properties that indicate the elastic and inelastic behavior of a material when it is subjected to a force. Some of the commonly measured mechanical properties include the Young's modulus, yield strength, ultimate tensile strength, shear modulus, work hardening coefficients and hardness numbers. The mechanical properties provide the basic design information on the strength of materials and for the specification of materials. These properties are typically measured by tensile tests, compression tests and the hardness tests.

1.1 Tensile test

The tensile test is the most widely used test in determining the mechanical properties of materials. In these tests, a specially prepared specimen is subjected to continuously increasing uni-axial tension force. The elongation of the material is measured simultaneously. A typical stress-strain curve is shown in Figure 1-1.

This thesis follows the style and format of ASME *Journal of Manufacturing Science and Engineering.*

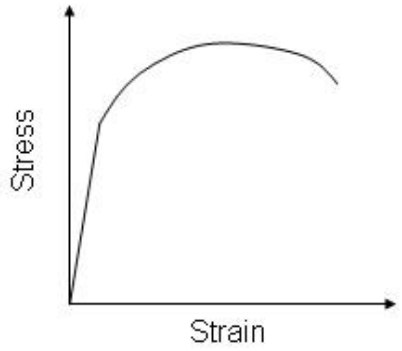

Figure 1-1: Typical engineering stress-strain curve

1.1.1 Engineering stress-strain curve

The curve so obtained from the tensile test is called the engineering stress-strain curve. The engineering stress and strain are given by

$$S = \frac{P}{A_0} \tag{1-1}$$

$$e = \frac{\Delta l}{l_0} \tag{1-2}$$

where e is the engineering strain

S is the engineering stress

Δl is the change in length

A_0 is the original cross-section area of the specimen

l_0 is the original length of the specimen

At the beginning of the test, the material extends elastically during which if the load is released, the sample returns to its original length. The material is said to have passed its

elastic limit when the load is sufficient to initiate plastic or non-recoverable deformation. On further loading, the stress to produce continued plastic deformation increases with increasing plastic strain, i.e., the metal strain-hardens. The stress reaches a maximum at the ultimate tensile strength. At this point necking begins and the engineering stress decreases with further strain until the material fractures. Figure 1-2 shows a typical tensile testing machine.

Figure 1-2: Tensile testing machine

1.1.2 True stress-strain curve

The engineering stress-strain curve does not give a true indication of the deformation characteristics of a metal because it is based on the initial dimensions of the specimen,

and these dimensions change continuously during the test. If the stress is measured from the instantaneous cross-sectional area associated with a particular load rather than the original stress, then it is called the true stress. True stress is defined as the ratio of the load on the sample to the instantaneous minimum cross-sectional area supporting that load.

$$\sigma = \frac{w}{A_i} \tag{1-3}$$

where σ is the true stress

w is the load on the sample.

A_i is the instantaneous minimum cross-sectional area supporting the load w.

True strain is defined as the integral of the ratio of an incremental change in length to the instantaneous length of the sample.

$$\varepsilon = \int_{l_0}^{l_i} \frac{dl}{l} \tag{1-4}$$

where l_0 is the initial length

l_i is the instantaneous length

By integrating equation 1-4,

$$\varepsilon = \ln\left(\frac{l_i}{l_0}\right) \tag{1-5}$$

The curve so obtained from the true-stress and true-strain plot is also called the flow curve since it represents the basic plastic-flow characteristics of the material. Figure 1-3 compares the engineering and true stress-strain curves.

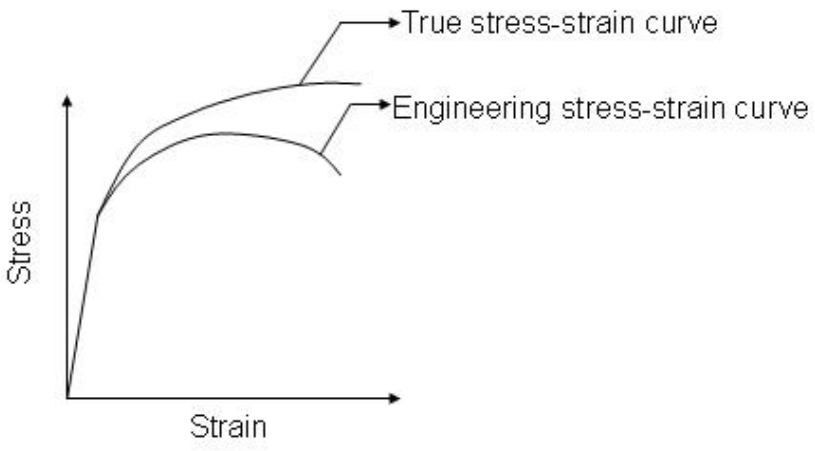

Figure 1-3: Engineering and true stress-strain curves

For most ductile metals that have not been cold worked, the behavior from initial yield to ultimate load is adequately described by an expression of the form

$$\sigma = K\varepsilon^n \tag{1-6}$$

where ε is the true strain

σ is the true stress

K is the work hardening constant

n is the work hardening exponent

The relation between the engineering stress-strain curve and the true stress-strain curve is given by

$$\varepsilon = \ln(1+e) \tag{1-7}$$

$$\sigma = S(1+e) \tag{1-8}$$

1.2 Hardness test

Hardness test is the second most common test that is used to evaluate mechanical properties. Hardness is defined as the ability of one material to scratch another material or the resistance to indentation. The indentation hardness is the most commonly used form of hardness. Spherical, conical or pyramidal indenters have been used for the indentation hardness tests. There are three principal standard test methods for expressing the relationship between hardness and the size of the impression namely Brinell, Vickers, and Rockwell. Figure 1-4 shows a typical Brinell hardness tester.

Figure 1-4: Brinell hardness tester

The hardness tests have certain restrictions and disadvantages. For example, no scale, in the most simple and commonly used indentation hardness, the Rockwell hardness, adequately spans the whole range of materials used in the sheet metal industry. Also, each scale has a minimum thickness needed to avoid the anvil effect i.e. the effect of substrate or support on the observed hardness [22]. The advantages of indentation hardness techniques are that they are less destructive than tensile test, quick, and can be applied to small material samples and localized in fashion. On the other hand, tensile tests are usually time consuming, destructive and need specially prepared specimens. Figure 1-5 shows a specimen for tensile testing.

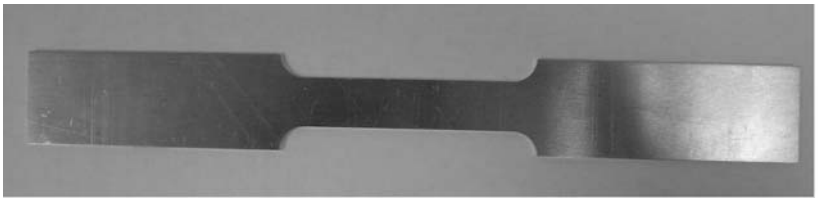

Figure 1-5: Tensile coupon

1.3 Research objective

The objective of the proposed research is to develop a methodology to determine mechanical properties of a material by indentation techniques. A series of indentations will be made on the specimen with a spherical indenter with different loads. Figure 1-6 shows a series of indentation formed from different loads. The diameter of the

indentation will be related to the load applied to determine the mechanical properties of the material, namely the yield strength and the work hardening parameters.

Tensile tests give the stress-strain behavior of materials. However they are destructive and time consuming. Even though hardness tests are less destructive and easy, they do not present the stress-strain behavior of the material behavior, which is preferred over hardness numbers. The present method combines the advantages of both the tensile testing and the hardness testing techniques. The elasto-plastic properties of a material can be determined quickly without having to prepare specimens or destroy them.

Figure 1-6: Multiple spherical indentations on metal surface

To implement the proposed methodology in a production line like a sheet metal processing line, the diameter of the indentation needs to be measured quickly. Hence a new fiber optic sensing technique to determine the diameter of the indentation will be built and tested. A semiconductor laser beam will be used to characterize the diameter of the indentation. An incident light beam will be coupled back into an optical fiber upon

reflection from the metal surface. It is proposed that, by measuring the diffused light power reflected from the metal surface, the diameter of the indentation can be measured.

The spherical indentation technique is difficult for real time mechanical property measurement of sheet metal in a processing line. Problems arise as the strip is traveling at 2,000 to 4,000 ft/min (10,000 to 20,000 mm/sec) in the processing line. As a first step in developing a process that could be implemented in a real time processing line, the feasibility of using laser shock processing will be investigated.

It is proposed to study three materials: copper, nickel and aluminum. To simulate the process numerically, commercially available software, ABAQUS, will be used to predict the material deformation for different laser intensities. The depth of the indentation will be a function of the material response to high pressure and strain rate. The deformation of three materials for different laser intensities will be studied and the parameters affecting the depth of the indentation will be identified.

2. LITERATURE REVIEW

The spherical indentation method can be used to determine the elasto-plastic properties of the material. There are different ways in which the stress-strain curve can be determined from the spherical indentation tests.

Three types of relation between the indentation parameters can be considered:

- Mean pressure – contact radius relation, $P_{avg} \sim (a/D)$
- Force – contact radius relation $w \sim (a/D)^{n+2}$
- Force – penetration depth relation $w \sim (h_i/D)^{n/2+1}$

where P_{avg} is mean pressure, w is force, D is ball diameter, a is the radius of the indentation, h_i is penetration depth, and n is work hardening exponent. [4]

One of the methods of measuring mechanical properties is by observing the geometry of the indentation after unloading. A considerable amount of work has been done to determine the flow properties of the material from the spherical indentation tests. Meyer and Tabor [25] did the earliest work in this field. Meyer proposed that the relation between the load and the indentation diameter follow a power law.

$$w = Md^m \tag{2-1}$$

where M and m are material constants. Tabor [25] showed a direct relation between the indentation radius, a, ball diameter, D and the plastic strain. He also showed the mapping between the stress, σ and the average pressure, P_{avg}.

Norbury and Samuel [18] studied the elastic recovery on unloading and sinking-in or piling- up of different materials in the Brinell hardness test. Atkins et al. [4] conducted indentation tests with a diamond cone on copper and mild steel and have determined a relationship between the hardness, cone angle and the yield stress. Cahoon et al. [5] have determined the yield strength, ultimate strength and the strain hardening coefficient from indentation hardness tests. Diamond pyramid hardness has been used to estimate the parameters. Rickerby [20] studied the elastic recovery in spherical indentations after unloading for large diameters of indentation and large loads.

Shabel et al. [22] used the modified Meyers hardness taking into account the machine deflection and the spring-back effect after the load was removed. They assumed that the net plastic strain ε_p is proportional to the quantity (d/D^*) where D^* is the relaxed radius of curvature of the impression and d is the impression diameter. The modified Meyer equation has been used for further analysis. Shabel [23] developed a procedure for converting Rockwell hardness numbers between the normal and the superficial scales.

Hill et al. [11] demonstrated that the relation between the mean pressure and the contact radius is of the from

$$P_{avg} = \frac{w}{\pi a^2} = \alpha \beta^n K \left(\frac{a}{D} \right)^n$$

where α and β are universal constants with values of 2.8 and 0.4 respectively,

K is the work hardening coefficient

n is the work hardening exponent

Alcala et al. [2] measured the piling up and sinking of materials around Vickers and spherical indentation of metals and ceramics in the unloaded state and have correlated with the strain hardening exponent n.

Kucharski's et al. [14, 15] procedure of identifying the plastic hardening parameters, K and n requires the specification of three indentation parameters namely, the depth of penetration in the loaded state h_t, the depth of penetration in the unloaded state h_p and the loading force w. The loading force is measured in the loaded configuration while the indentation radius is determined in the unloaded configuration and is then divided by the diameter of the indentation meniscus in a loaded state. Thus the method does not consistently refer to one configuration and the effect of elastic unloading is neglected.

The load-displacement curve is one of the most common methods of measuring mechanical properties by spherical indentation. This is also known as the continuous indentation test. The displacement of the indenter is recorded for various loads during loading and unloading. From the load-displacement curve of an indenter during indentation, the stress-strain curve may be established. The Young's modulus, for example, may be obtained from the peak load and the initial slope of the unloading curve [17].

Robinson et al. [21] determined the stress-strain curve for hardness together with curves for the Meyer stress, indentation diameter and ratio of elastic to plastic strain continuous indentation tests. Taljat et al. [26] proposed the maximum strain method and the minimum strain method for the calculation of the stress-strain curve. However, no specific method has been mentioned to determine the strain hardening exponent *n*. Zhao [30] determined the elastic-plastic stress-strain relation for polymeric thin films by combining the micro plane strain compression testing and FEA simulations. Cheng et al. [6] used dimensional analysis and finite element calculations to derive simple scaling relationships between the loading and the unloading curve, contact depth and hardness. With these relationships, the mechanical properties are determined.

Herbert et al. [10] identified a curved shape that terminates a small plateau from the graph drawn between the displacement and the ratio of contact depth to total depth. They identified this as the upper and the lower limits of displacement. From this limit they established a range for yield strength using Tabor's [25] relation that at the time of yielding. Nayebi et al. [17] used an indentation device to measure the force-displacement curve. They have used two functions that depend on the yield stress, σ_y, and the strain hardening exponent *n*. These functions have been deduced from the analysis of results obtained by finite element simulations on a series of metals.

Huber et al. [12] used neural networks to determine the material parameters from the data obtained from the spherical indentation. The required data sets were generated from

finite element simulations. Ma et al. [16] computed the Young's modulus and the stress-strain curve in the plastic region from the combination of the both spherical indentation test as well as from a series of finite element analysis. They have established an iterative procedure to determine the stress-strain curve. Clough et al. [8] measured the hardness of metals using a dropped ball by considering the strain rate effect on cold-rolled plain carbon (1018) steel.

Laser shock processing (LSP) has been widely used to increase the compressive residual stresses in the material. LSP does not involve the direct heating of the metal surface, but rather, involves directing a laser beam pulse onto an opaque overlay applied to the area being treated. A portion of the overlay is vaporized when the laser beam pulse hits it, creating an expanding gas release, which is further heated by the laser pulse. A pressure-induced shock, or stress, wave created at the surface is transmitted through the metal. A compressive residual stress is produced when the maximum stress of the shock wave exceeds the dynamic yield strength of the metal. This technique was patented in 1974 by Battelle Laboratory (Columbus, OH) researchers (US 1982000378975).

Clauer et al. [7] considered the hydrodynamic equations governing the evolution of pressure at the metal surface. Fabbro et al. [9] made a physical study of the laser shock processing and developed a model that assumes that, the laser irradiation is uniform and therefore shock propagation is one dimensional. Peyre et al. [19] developed a model to predict the plastically affected depths and compressive stresses during laser shock

processing. Thorslund et al. [27] developed a model to predict the temperatures, pressures and stresses during laser shock processing. Zhang et al. [29] developed a constitutive model to predict the material behavior during laser shock processing by taking into account the effect of ultra high pressures and strain rate.

Zhang et al. [29] demonstrated that during laser shock processing, the target experiences pressures exceeding their dynamic yield strength inducing plastic deformation. The indentation produced on the target is a result of plastic deformation. In the current work, a preliminary study has been conducted to determine the mechanical properties of the material from the depth of the indentation. The deformation of three materials for different laser intensities has been studied and the parameters affecting the depth of the indentation have been identified.

3. METHODOLOGY FOR MECHANICAL PROPERTY MEASUREMENT BY MULTIPLE SPHERICAL INDENTATIONS

An indentation formed by a spherical indenter causes the material around the indentation to be displaced and increases the stress around the indentation. Let a force, *w* be applied on a spherical indenter of diameter *D*. Let the chordal diameter of the indentation be *d=2a*. Let the average pressure be P_{avg}. It is assumed that there is no friction between the surface of the indenter and the indentation.

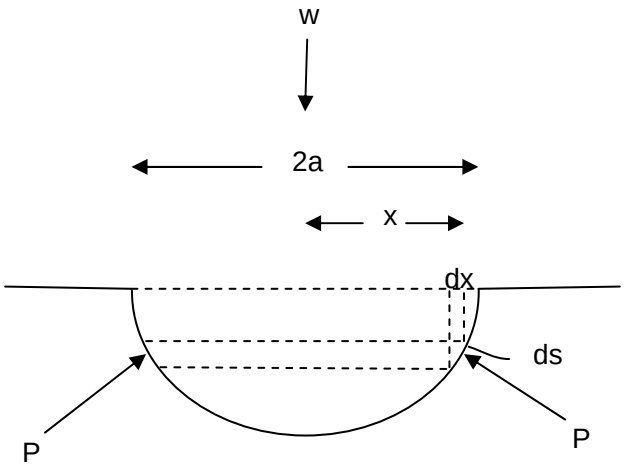

Figure 3-1: Calculation of mean pressure [25]

Figure 3-1 shows an indentation formed from a spherical indenter and the calculation of mean pressure. Consider the forces on an annulus of radius *x* and width *ds*. The area of the annulus lying on the surface of the indentation is $2\pi xds$ and hence the net force is $P_{avg} 2\pi xds$. By symmetry, the horizontal component of this force is zero while the

vertical component is $P_{avg} 2\pi x dx$. Taking the sum over the whole surface area of the indentation, the resultant vertical force, which is equal to *w*, is given by [25]

$$\begin{aligned} w &= \int_0^a P_{avg} 2\pi x dx \\ &= P_{avg} \pi a^2 \end{aligned} \tag{3.1}$$

Hence the average pressure is give by

$$P_{avg} = \frac{w}{\pi a^2} \tag{3.2}$$

where *w* - load applied in Newtons

a - chordal radius of the indentation in meters

3.1 Relation between mean pressure and stress

Tabor conducted out indentation experiments to measure the stress of the deformed material around and in the indentation. He observed that the stress in the material gradually rises as the edge of the indentation is approached. However, the empirical tests conducted by Tabor suggested that the stress at the edge of the indentation could be used as the 'representative' value for the whole of the deformed material around the indentation. Tabor conducted experiments over a wide range of materials and observed that the mean pressure is directly proportional to the stress in the indentation.

$$\begin{aligned} P_{avg} &\propto \sigma \\ P_{avg} &= c\sigma \end{aligned} \tag{3.3}$$

The value of '*c*' was found, on an average for aluminum to be 2.8.

$$P_{avg} = 2.8\sigma \tag{3.4}$$

where P_{avg} is the average pressure

σ is the stress in the indentation

Tabor observed the strain corresponding to this stress and found that the strain was proportional to the ratio *d/D* where *d* is the chordal diameter of the indentation and *D* is the diameter of the indenter.

$$\varepsilon = \psi \times \left(\frac{d}{D} \right) \tag{3.5}$$

Experimentally, the value of ψ was found to be 0.2.

$$\varepsilon = 0.2 \times \left(\frac{d}{D} \right) \tag{3.6}$$

where ε is the strain

3.2 Real time mechanical property measurement methodology

It is proposed that multiple indentations, each with a different load, be made on the sheet. The chordal diameter *d*, of the indentation is measured by the fiber optic sensing technique online. Then equations (3.2), (3.4) and (3.6) were used to determine the stress-strain data points in the plastic region as follows.

1) Measure the chordal radius of the indentation by fiber optic sensing technique.

2) Calculate average pressure $P_{avg} = \frac{w}{\pi a^2}$

3) Calculate the stress from the average pressure $\sigma = \frac{P_{avg}}{2.8}$

4) Calculate the strain from the chordal radius of the indentation $\varepsilon = 0.2 \times \left(\frac{d}{D} \right)$

From the multiple indentations, each with a different load, the 'approximate' stress-strain data points are first plotted. The reason that it is called an approximate is that there could be errors in the measurement of the indentation diameter or even in the application of the load. Hence, an error reduction algorithm is designed to improve the accuracy of the measurement of the stress-strain curve.

3.3 Error reduction algorithm

All the points in the plastic region of the stress-strain curve of the material are related by the equation, $\sigma_i = K\varepsilon_i^{\,n}$. Here n is the work hardening exponent and K is the strain hardening coefficient. Let (σ_1, ε_1) and (σ_2, ε_2) be any two values obtained from the indentation experiments for a material. The stresses and strains are related by the equations

$$\sigma_1 = K\varepsilon_1^{\,n} \tag{3.7}$$

$$\sigma_2 = K\varepsilon_2^{\,n} \tag{3.8}$$

Dividing equation (3.7) by equation (3.8), we have

$$\frac{\sigma_1}{\sigma_2} = \left(\frac{\varepsilon_1}{\varepsilon_2} \right)^n \tag{3.9}$$

Taking natural logarithm for equation (3.9) on both sides,

$$\ln\left(\frac{\sigma_1}{\sigma_2}\right) = n \times \ln\left(\frac{\varepsilon_1}{\varepsilon_2}\right) \tag{3.10}$$

$$n = \frac{\ln\left(\frac{\sigma_1}{\sigma_2}\right)}{\ln\left(\frac{\varepsilon_1}{\varepsilon_2}\right)} \tag{3.11}$$

Since σ_1, ε_1, σ_2 and ε_2 are known, the value of n can be obtained from the above equation. Hence from x number of indentation tests conducted, there are x points of stress and corresponding strain. From these x sets of data, following the above procedure, xC_2 values of n can be obtained. This data set that contains the values of the strain hardening exponents n are then fed to the *error reduction algorithm*, a code written in MATLAB.

3.3.1 Determination of strain hardening exponent 'n'

The algorithm first removes the outliers in the distribution of the data set of strain hardening exponent *n,* i.e., the algorithm determines the region where most of the values of n in the data set are concentrated and values that lie outside this region are ignored. This is done by a sorting algorithm. An appropriate tolerance limit is set for the algorithm. In the present study the tolerance limit was set as ± 0.05. The sorting algorithm assumes the first value of n in the data set as the reference value. The scatter in the vicinity of the region is determined.

A data point is said to lie in the vicinity region of the reference value if it lies with in the tolerance limit. The process is iterated by assuming all the points in the data set as the reference value. Then the region which is most populated is identified. In the current study, to qualify as the most populated region, the region should contain a minimum of 70% of the values in the data set. If there exists no region that meets this criterion, then it is suggested to take more samples and follow the methodology outlined.

Once this region is identified, a point which represents the distribution in the region is calculated. i.e. the mean of all the points in the region is determined. This value, n_f, is the work hardening exponent of the material and is used for further calculations in determining the values of the work hardening coefficient and yield strength of the material.

3.3.2 Determination of strain hardening coefficient *K*

To determine the strain hardening coefficient of the material, the value of *n* (from the set of data obtained from different loads) that is closest to n_f is identified. Let the stresses and strains corresponding to this value of *n* be (σ_1, ε_1) and (σ_2, ε_2). The value of the strain hardening coefficient *K* is obtained as follows.

1) Let $K_1 = \dfrac{\sigma_1}{\varepsilon_1^{\,n_f}}$

2) Let $K_2 = \frac{\sigma_2}{\varepsilon_2^{n_f}}$

3) The strain hardening coefficient K is the mean of K_1 and K_2.

$$K = \frac{K_1 + K_2}{2} \tag{3.12}$$

The stress-strain curve of the material in the plastic region is plotted from the equation $\sigma = K\varepsilon^{n_f}$. The yield strength of the material is then determined from the following equation. [36]

$$K = \frac{\sigma_y}{\left[\frac{\sigma_y}{E} + 0.002\right]^{n_f}} \tag{3.13}$$

where σ_y is the yield strength of the material

E is the Young's modulus of the material

3.4 Mechanical indentation experimental results

3.4.1 Experimental procedure

Indentation tests were conducted on an aluminum bar of thickness 25.4 mm. Five indentations were made on the aluminum block with a Brinell hardness tester. The diameter of the indenter D was 10 mm. Different loads were applied to the material and indentation diameters d were observed under the microscope. The results are shown in the Figure 3-2.

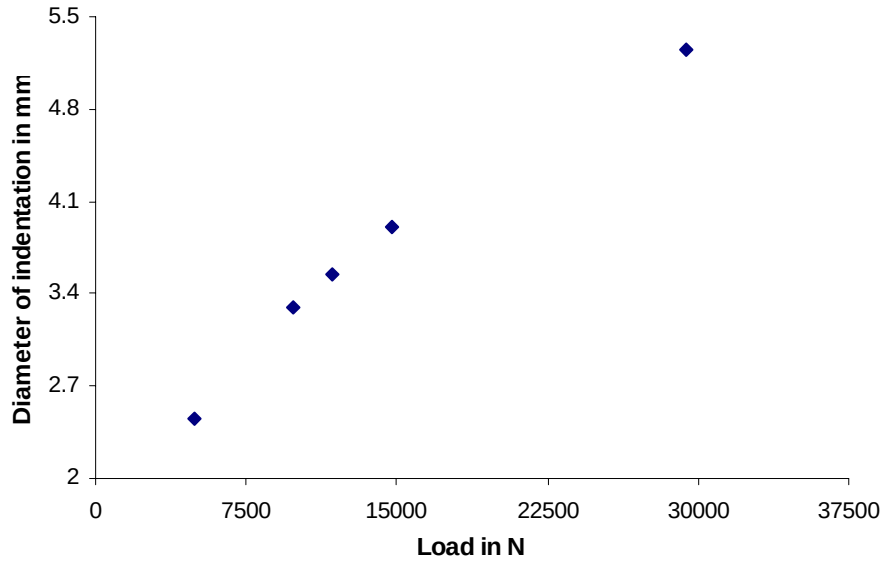

Figure 3-2: Diameter of the indentation for various loads

Tensile coupons were cut out from the same block and tested. The stress-strain curve of the material obtained from the tensile test is shown in Figure 3-3.

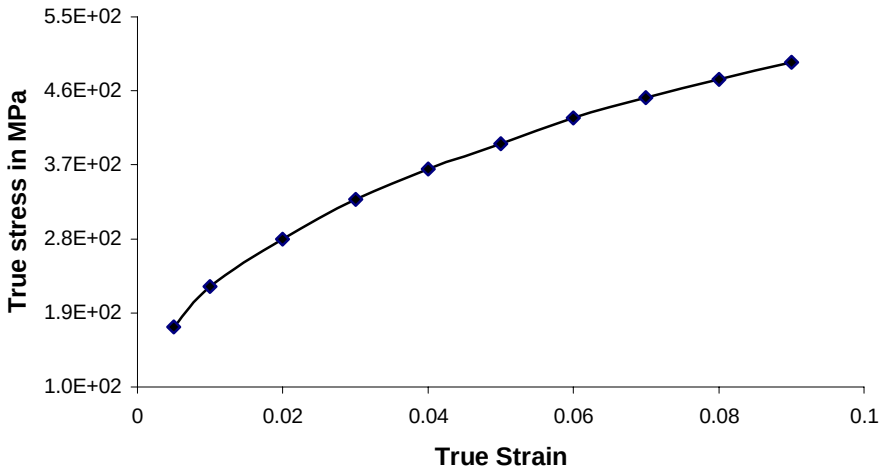

Figure 3-3: Stress-strain curve of material from tensile test

The procedure outlined in the previous section was followed and the approximate stress-strain data points obtained is shown in the Figure 3-4.

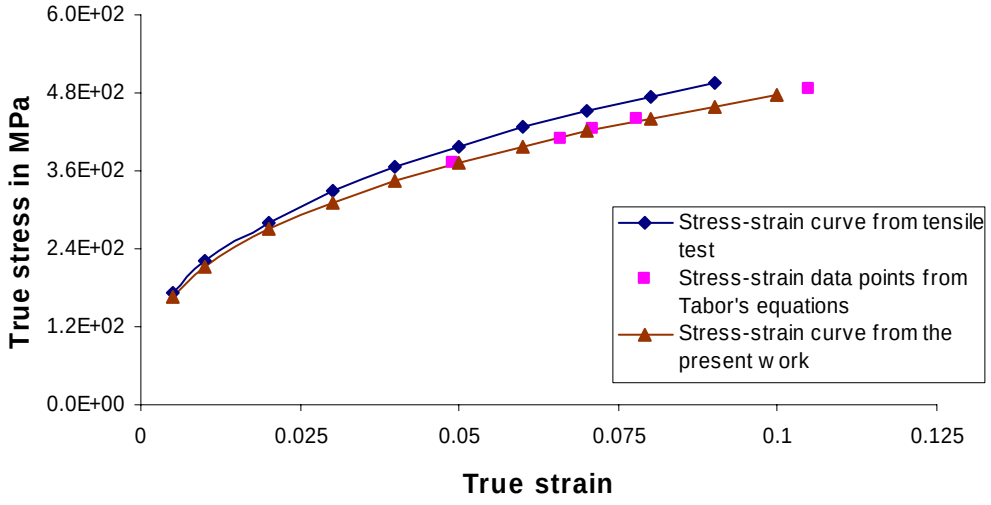

Figure 3-4: Comparison of stress/strain curves from experimental results

The values of the strain hardening exponent n and strain hardening coefficient K were calculated to be 0.3547 and 1080.6 MPa respectively. Figure 3-4 compares the stress-strain curve from the tensile test and stress-strain curve defined by the equation $\sigma = K\varepsilon^n$.

The calculated yield strength of the material experimentally was found to be 154 MPa while the yield strength from the tensile test was found to be 163.3 MPa. It is seen that the results obtained are in close agreement with the expected results.

3.5 Finite element analysis of mechanical indentation process

Efforts were made to investigate this method numerically. To further demonstrate this technique and to validate this methodology for different aluminum alloys, a finite element code of the mechanical indentation process was developed. The code was first validated with the experimental results from the previous chapter and was extended for different aluminum alloys namely, 3004-O, 6063-T6 and 6063-O.

3.5.1 Finite element modeling

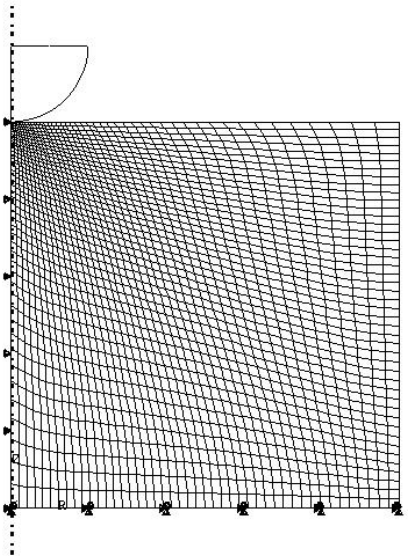

Figure 3-5: Finite element model

An axi-symmetric finite element model was developed to computationally simulate the spherical indentation experiment. The spherical indenter is modeled as a rigid body. The

influence of friction at the interface between the indenter and the specimen was neglected. The meshing was denser in the top-left region where the material is expected to deform while a coarse mesh is used in the other regions. This was done to decrease the computation time and increase efficiency. The plastic constitutive behavior was modeled by defining the stress-strain points in the power law curve, $\sigma = K\varepsilon^n$. Von-Mises yield criterion is assumed. A cylindrical coordinate system with radial coordinate, r, and axial coordinate, z was used in all models. The bottom surface was constrained in all directions while the centerline surface is constrained in the r direction. The geometry and the boundary conditions for the developed model are shown in Figure 3-5.

The simulation was modeled in two steps. The indentation process, the first step, was performed by an ABAQUS Explicit code while the process of elastic recovery was modeled in the ABAQUS Standard by importing the results from the first step. The simulation time for the first step was 1 ms while for the second step it was 100 ms. Figure 3-6 shows the deformed shape of the developed finite element model.

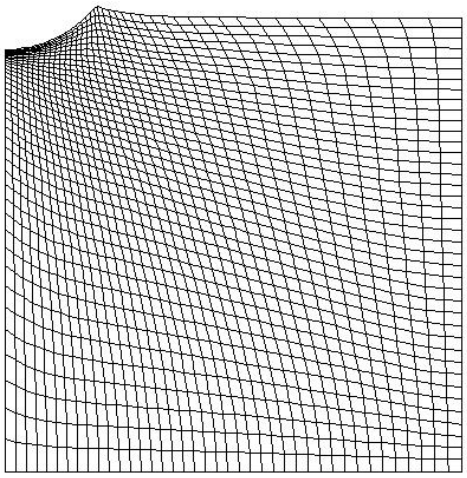

Figure 3-6: Deformed finite element model of spherical indentation

3.5.2 Verification of the FEA model

The developed FEA model was verified by comparing the results obtained from the experiments. The diameter of the indentation was the criteria used for the comparison of the results. The stress-strain curve of the material obtained from the tensile tests was used to model the material behavior. To determine the density of the material, a bar of material was weighed and is divided by its volume. Figure 3-7 compares the indentation diameter for various loads, calculated numerically from the simulation, with the results from the experiments.

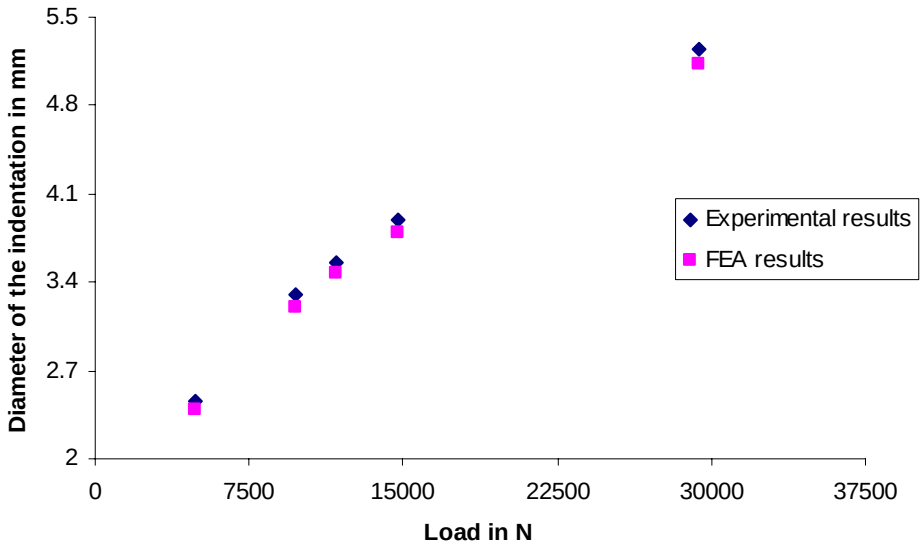

Figure 3-7: Comparison of FEA and experimental results for diameter of indentation

As seen, the results from the FEA model are in close agreement with the experimental results. Hence the validity of the FEA model is established.

3.5.3 Results from FEA

Figure 3-8 compares the stress-strain curve obtained from the indentation experiments and the FEA model. The values of strain hardening exponent n and strain hardening coefficient K calculated to be 0.3473 and 1121 MPa respectively.

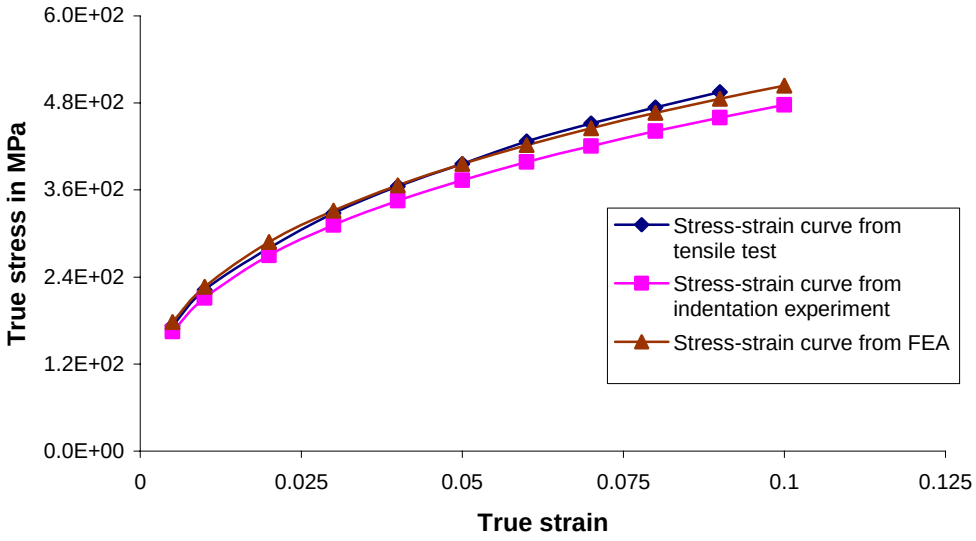

Figure 3-8: Comparison of stress-strain curves from experiment and FEA

The calculated yield strength of the material from FEA is 169 MPa while the yield strength from the tensile test was 163.3 MPa. It is seen that the results obtained are in close agreement with the expected results.

The verified FEA model was then used to test a variety of Aluminum alloys. The standard stress-strain curve of the alloy from ASM metals reference book [3], was used to model the material behavior in the FEA model. Five different loads were applied to the material with the spherical indenter. From the diameter of the indentations, the stress-strain curve and the yield strength were back-calculated using the procedure discussed in the previous section. The back-calculated stress-strain curve was compared

with the curve input to the FEA. The results of various aluminum alloys are shown in the following Figures 3-9, 3-10 and 3-11.

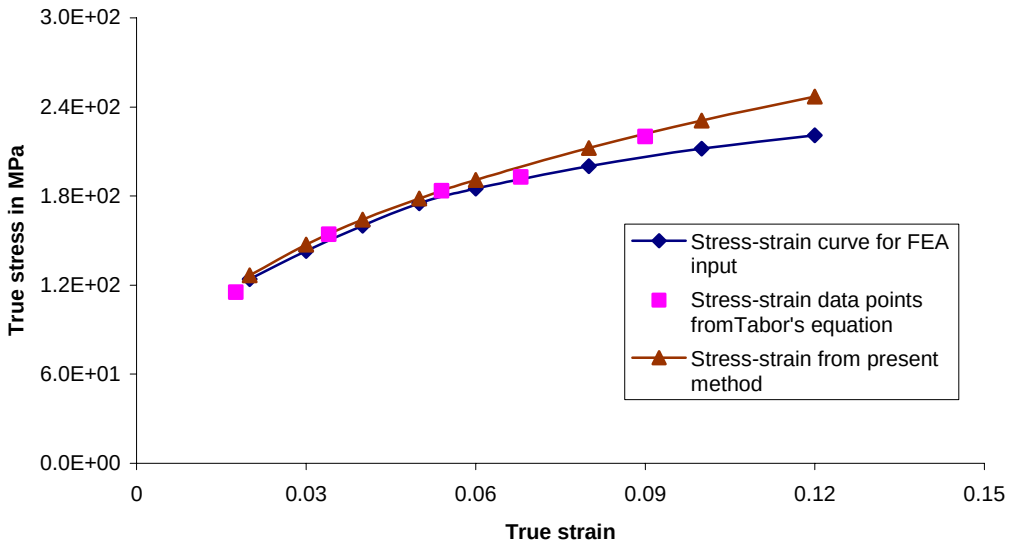

Figure 3-9: Comparison of stress-strain curves for 3004-O

The calculated yield strength of 3004-O was found to be 61.8 MPa while the theoretical yield strength was 67 MPa.

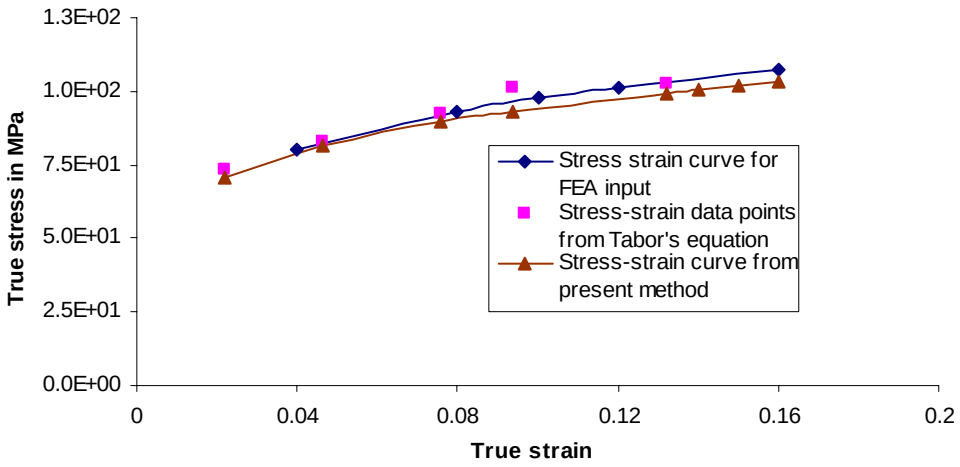

Figure 3-10: Comparison of stress-strain curves for 6063-O

The calculated yield strength of 6063-O was found to be 47.05 MPa while the theoretical yield strength was 48.3 MPa.

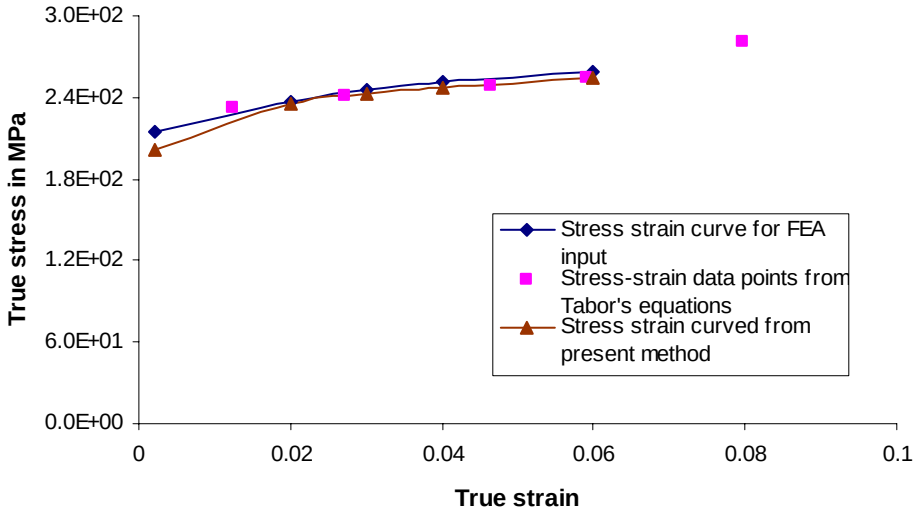

Figure 3-11: Comparison of stress-strain curves for 6063-T6

The calculated yield strength of 6063-T6 was found to be 214.83 MPa while the theoretical yield strength was 214 MPa. Table 3-1 compares the results obtained from the developed methodology with the theoretical values for different alloys.

Table 3-1: Summary of results for spherical indentation

Material	*Theoretical value of n*	*Calculated value of n*	*Theoretical value of K (MPa)*	*Calculated value of K (MPa)*	*Theoretical value of σ_y (MPa)*	*Calculated value of σ_y (MPa)*
3004-O	0.367	0.3732	521.9	545.2	67	61.8
6063-O	0.2	0.1929	154.12	147	48.3	47.05
6063-T6	0.08	0.0688	324.09	308.83	214	214.83

3.6 Discussion

It is found from the above results that the proposed technique of determining the mechanical properties of the materials gives accurate results. However, it must be mentioned that the proposed technique tends to become relatively inaccurate as the strain hardening exponent *n* approaches zero. This is because the difference in values of the indentation diameters is less for a material whose value of *n* is close to zero compared to a material with a higher value of *n* for the same applied loads.

Let a_1 and a_2 be the radius of the indentations formed by applying two different loads w_1 and w_2 on a material whose work hardening constant is n_1. Similarly let a_3 and a_4 be the radius of the indentations formed by applying two different loads w_1 and w_2 on a material

whose work hardening constant is n_2. Let $n_1 < n_2$ and n_1 very close to zero. Let $w_1 < w_2$. Hence $a_1 < a_2$ and $a_3 < a_4$.

It is known that for n_1 less than n_2, the stress-strain graph is as shown in Figure 3-12.

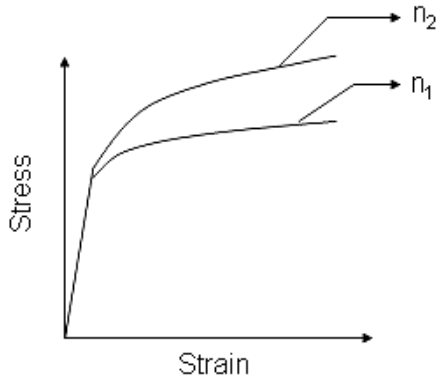

Figure 3-12: Stress-strain graph of materials with different work hardening exponents

Let

$$\sigma_1 = \frac{w_1}{2.8 \times \pi \times a_1^{\,2}} \tag{3.13}$$

$$\sigma_2 = \frac{w_2}{2.8 \times \pi \times a_2^{\,2}} \tag{3.14}$$

Dividing equation (3.14) by equation (3.13)

$$\frac{\sigma_2}{\sigma_1} = \frac{w_2}{w_1} \times \left(\frac{a_1}{a_2} \right)^2 \tag{3.15}$$

Since the first material work hardens to a small extent, we have

$$\frac{\sigma_2}{\sigma_1} \approx 1 \tag{3.16}$$

Rearranging equation (3.15)

$$\frac{w_1}{w_2} = \left(\frac{a_1}{a_2} \right)^2 \tag{3.17}$$

Writing similar equations for the second material

$$\sigma_3 = \frac{w_1}{2.8 \times \pi \times a_3^{\,2}} \tag{3.18}$$

$$\sigma_4 = \frac{w_2}{2.8 \times \pi \times a_4^{\,2}} \tag{3.19}$$

Dividing equation (3.19) by equation (3.18)

$$\frac{\sigma_4}{\sigma_3} = \frac{w_2}{w_1} \times \left(\frac{a_3}{a_4} \right)^2 \tag{3.20}$$

But the second material work hardens appreciably and hence

$$\frac{\sigma_4}{\sigma_3} > 1 \tag{3.21}$$

$$\frac{w_1}{w_2} < \left(\frac{a_3}{a_4} \right)^2 \tag{3.22}$$

Comparing equations (3.17) and (3.22)

$$\left(\frac{a_1}{a_2} \right) < \left(\frac{a_3}{a_4} \right) \tag{3.23}$$

It is observed from the equation (3.23) that as the value of the strain hardening exponent tends to zero the difference in diameter of the indentations decreases. When the value of n is close to zero, very accurate measurement of the indentation diameter is needed. Errors in the measurement of the diameter of the indentation may lead to less accurate results.

4. FIBER OPTICS SENSING TECHNIQUE

The developed methodology of determining the mechanical property by multiple spherical indentations requires frequent measurement of the indentation diameter. Use of a microscope to measure the diameter of the indentation would defeat the very purpose of the developed methodology – quick measurement of mechanical properties. To further implement this process in a production line like a sheet metal processing line, quick measurement of the indentation diameter is a necessity. To meet this requirement, a fiber optics sensing technique has been developed to measure the indentation diameter.

A semiconductor laser beam was used to characterize the diameter of the indentation. An incident light beam was coupled back into an optical fiber upon reflection from the metal surface. By measuring the diffused light power reflected from the metal surface, the diameter of the indentation was measured.

4.1 Introduction to fiber optics

Fiber optics use light pulses to transmit information down fiber lines. The difference in refractive index causes the total internal reflection that guides the light through the core. The structure of the optical fiber is shown in Figure 4-1. The “light guiding” core of the fiber is made of a material with higher refractive index than the cladding that surrounds it.

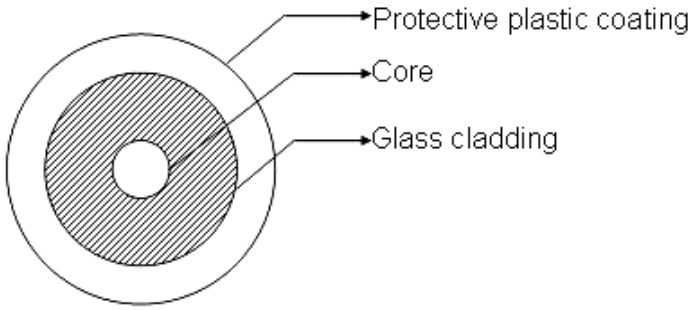

Figure 4-1: Cross section of optical fiber

4.2 Experimental setup

The fiber was first stripped from its plastic coating. The flatness on the fiber tip was obtained by cleaving with a cleaving tool. Then the cladding part and the core of the fiber was inserted inside a metal tube just for protection and secured with epoxy as shown in Figure 4-2.

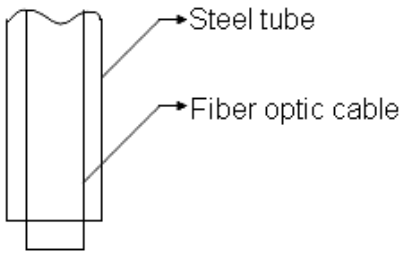

Figure 4-2: Fiber optic cable on sensing end

Since the fiber core was 10 μm whereas the approximate diameter of the indentation (from Alcoa sample) was about 500 μm, a magnification of 50X was used for the fiber beam spot to cover the indentation. A convex lens focused the spot onto the aluminum surface with adjustable magnification. The experimental setup shown in Figure 4-3 includes a passive coupler and a semiconductor laser.

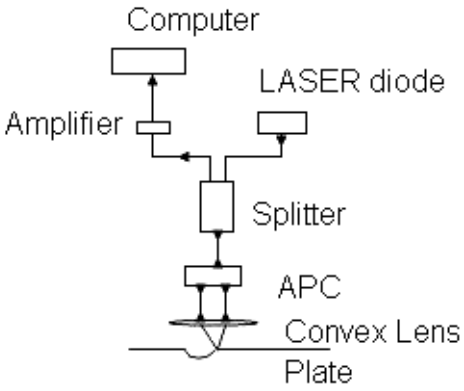

Figure 4-3: Experimental setup for fiber optics sensing technique

4.2.1 Initial experimental setup by rotating the specimen

In a sheet metal processing line, the strip travels at 2,000 to 4,000 ft/min. However, such high linear speeds cannot be simulated in laboratories when performing experiments. To demonstrate that signals can be obtained at high speeds, the specimen was rotated on a motor. As shown in Figure 4-4, a fixture was designed and assembled to position the fiber and a convex lens on top of a rotating aluminum sheet. The rotation motion was provided by the shaft of a motor. The setup allows the reflected light power signals to be collected for initial investigation.

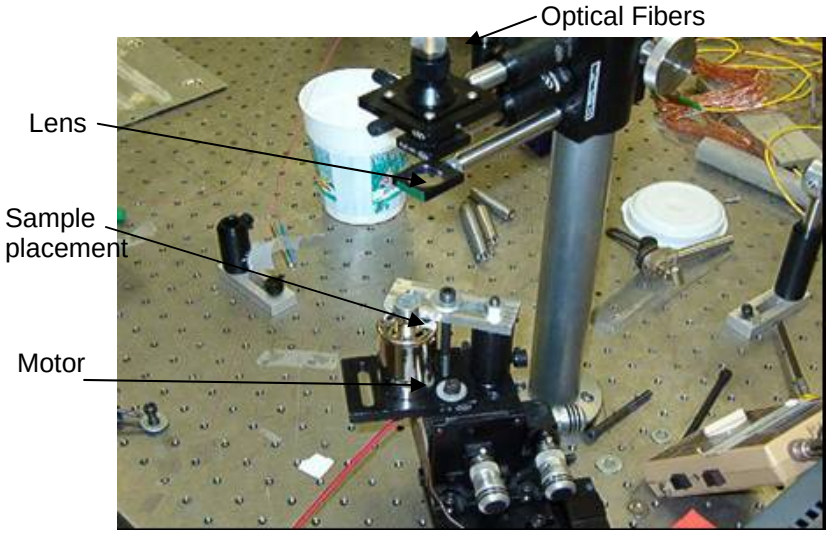

Figure 4-4: Initial experimental setup (rotational motion)

Aluminum sheets with indentations created from the Alcoa apparatus were cut into small samples. A mirror was placed on the surface of the specimen to produce the trigger signal as shown in Figure 4-5. While the specimen rotated in the counter-clockwise direction, the indentation signal followed the trigger signal. Figures 4-6 and 4-7 show the signals obtained from the experiments from deep and shallow indentations. The peak signal is the signal from the mirror. The encircled region is the signal obtained from an indentation. It is found that a larger/deeper indentation produces a lower reflective light intensity. This is reasonable since the shallow indentation reflects more light than the deeper indentation. The focus of the laser beam is on the flat surface. The deeper indentation would be more out of focus than the shallow indentation. By performing more experiments, it was observed that different indentations produce different signals. However, there are other unwanted signals not originating from the indentation as shown in Figures 4-6 and 4-7. The source of these unwanted signals was most probably the

inherent surface texture of aluminum as well as the internal reflection from the tip of the fiber.

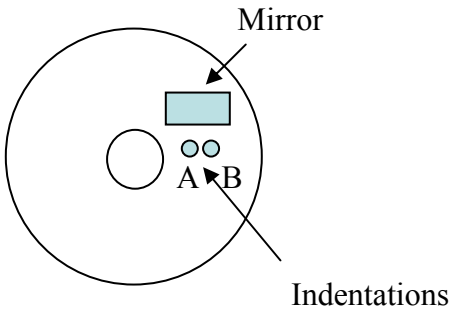

Figure 4-5: Specimen with indentations

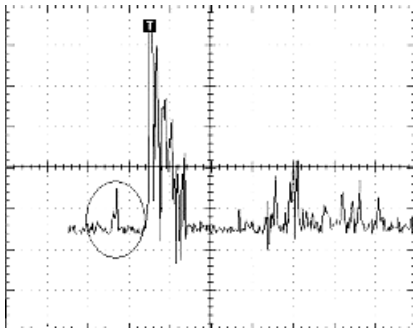

Figure 4-6: Signal from a deeper indentation

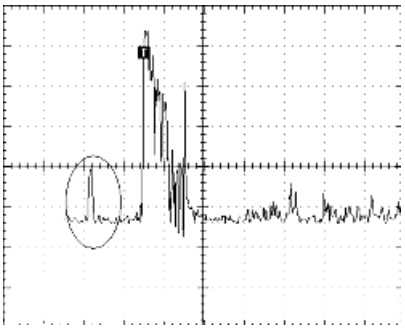

Figure 4-7: Signal from a shallow indentation

Further study suggested that the surface texture of the aluminum sheet contributes significantly to the disturbances of the signal. Instead of a well-diffused light reflected from a random surface, as originally anticipated, the textured surface (parallel groves) produces an undesirable high intensity line that sweeps across the lens aperture. Although this signal can be related to the *roughness* of the strip and might be of interest in the future, it is undesirable in the current study. Another source of noise observed seems to originate from the reflected light from the flat tip of the fiber, causing the detector signal to fluctuate even if the specimen is stationary. This fluctuation may be due to some coherent mixing of reflected signals induced by changes in the laser spectrum (caused by strong optical feedback into the laser). The unwanted intensity variation was significant compared to that of the indentation as seen from Figure 4-6 and Figure 4-7.

4.2.2 Measuring indentation diameter in linear motion

In order to simulate actual conditions, the sample was moved linearly at a slow speed under the optical fiber with the help of a linear actuator. To reduce the disturbance cause by the reflection from the flat tip of the fiber, the fiber was replaced with an angle polish connector (APC) fiber. The APC fiber used has a 7° angle tip. As shown in Figure 4-8, the reflected light from the tip does not contribute to the signal collected from the detector and hence reduce the noise.

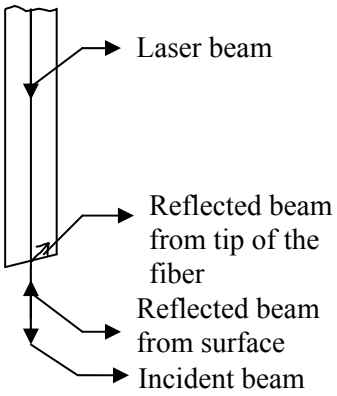

Figure 4-8: Angle polish connector optical fiber

To emulate the linear motion in a processing line, the measurements are taken from a specimen mounted on a linear actuator as shown in Figure 4-9. Two different size indentations were made in a straight line. Since no trigger signal was required, mirror was not attached to the specimen. Although signals taken from a production line will be along the rolling direction, crossing the ‘lines’ parallel to the rolling direction cannot be completely prevented. Considered as the worst case condition, the specimen was

arranged to travel in the transverse direction as shown in Figure 4-10. Due to experimental limitations, the linear motion was prescribed at 265 μm/s and the total travel distance was 18720 μm.

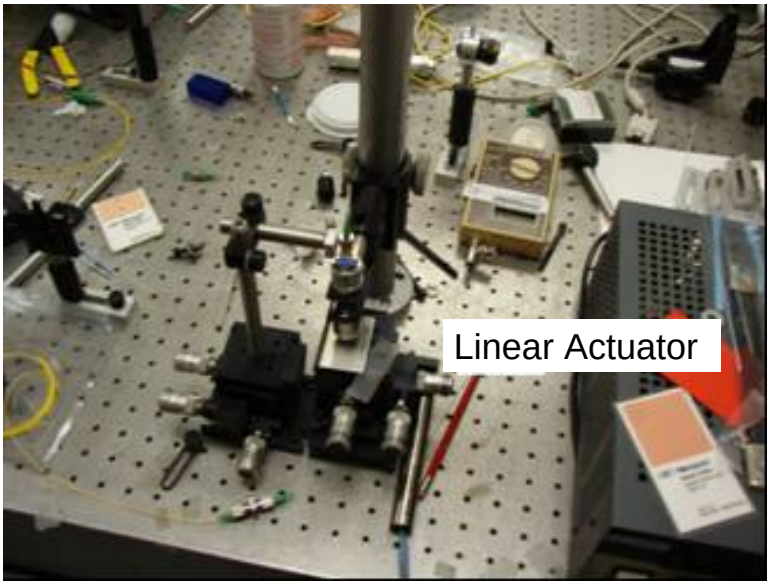

Figure 4-9: Linear motion experimental setup

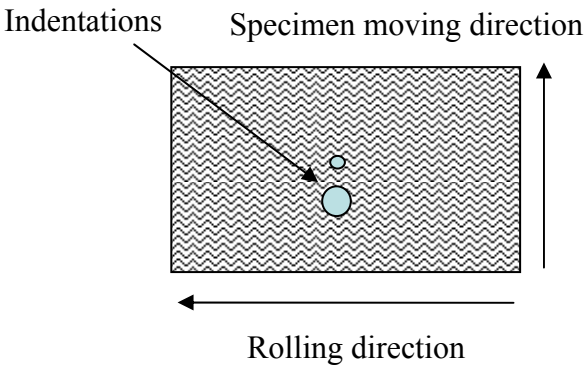

Figure 4-10: Specimen for linear motion indentation measurement

Figure 4-11 shows the signal collected from a specimen when the laser spot bypasses the indentation. Strong spatially dependent light power intensity due to surface texture was obtained. Figure 4-12 shows the signal received when the laser spot pass through two consecutive indentations. As the indentation is scanned by the semiconductor laser, the reflected beam from the indentation surface is scattered and is not coupled back. Hence low signal intensity was observed as the indentation was scanned be the semiconductor laser beam. It can be observed that the larger indentation results in wider width of low signal intensity than the smaller indentation. This width of low intensity is a measure of the diameter of the indentation.

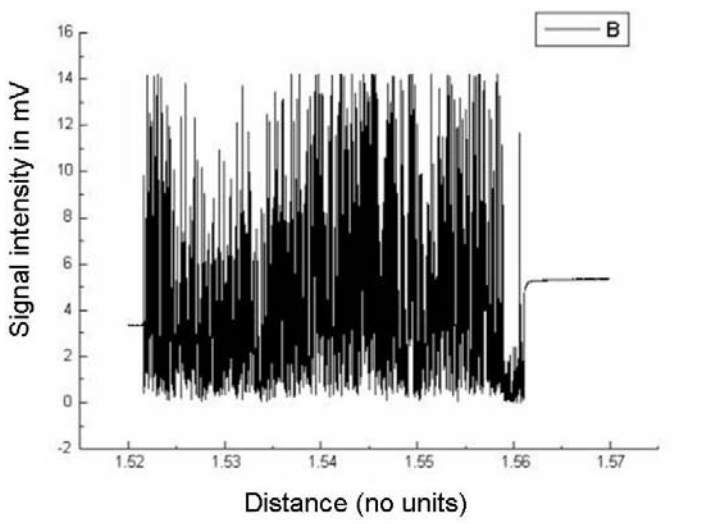

Figure 4-11: Signal from a specimen with no indentation
(travel distance of 18720 μm at 265 μm/s)

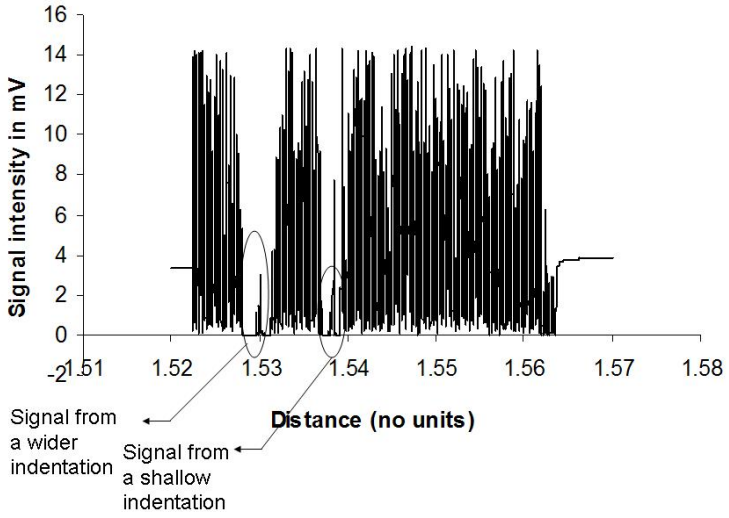

Figure 4-12: Signal from a specimen with two indentations
(travel distance of 18720 μm at 265 μm/s)

The short travel span and slow moving speed in the current experimental setup does not invalidate the conclusion drawn below when the movement is very fast since it is only a matter of increasing the sampling rate. Figure 4-13 shows that with the travel span reduced to 3700 μm, the indentation diameter (related to the indentation signal width) can be clearly identified. Figure 4-14 represents the surface texture signal from a flat surface when the travel span is 120 μm.

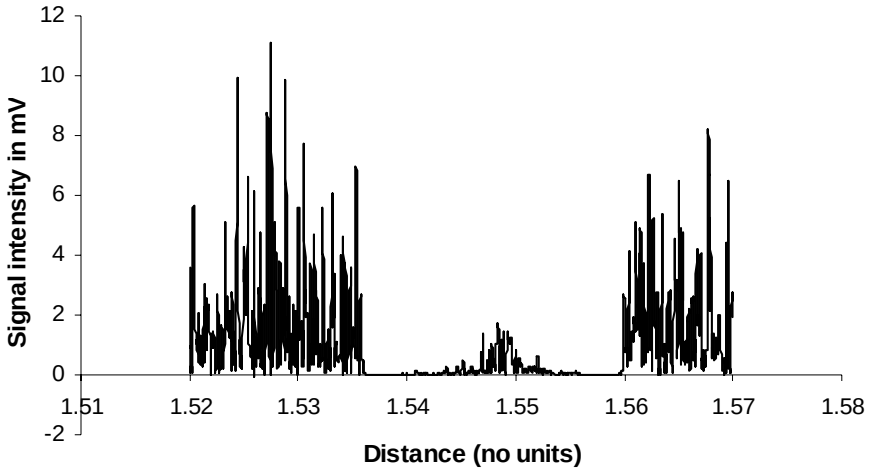

Figure 4-13: Signal of an indentation at a short travel span
(travel distance of 3700 μm at 53 μm/s)

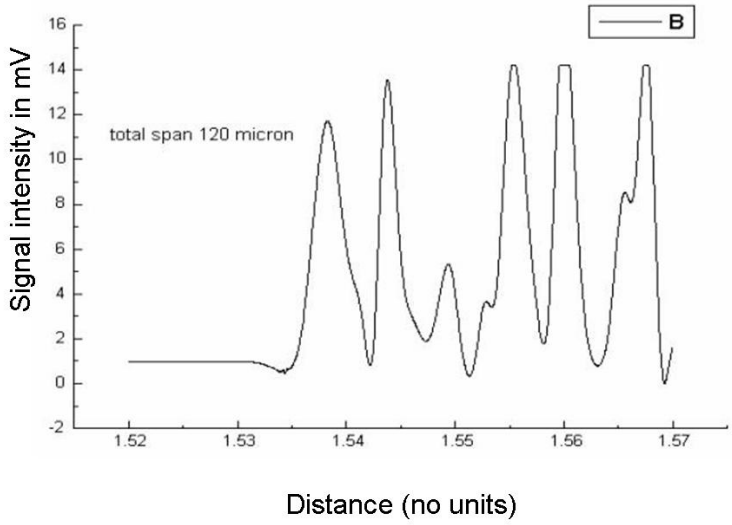

Figure 4-14: Surface texture signal at 120 μm travel span
(travel distance of 120 μm at 1.8 μm/s)

4.3 Results and discussion

Evaluating various indentations, it was observed that the measured width of low signal intensity is proportional to the indentation diameter (diameter observed from an optical microscope) as shown in Figure 4-15. Eight indentations of different diameter were made on an aluminum sheet with balls of diameter 2 mm. They were all translated with the same speed under the optical fiber. The width of the signals was plotted against the diameter of the indentations. The results are plotted in Figure 4-15. From the figure it is seen that there exits a linear relation between the width of the signal and the diameter of the indentation.

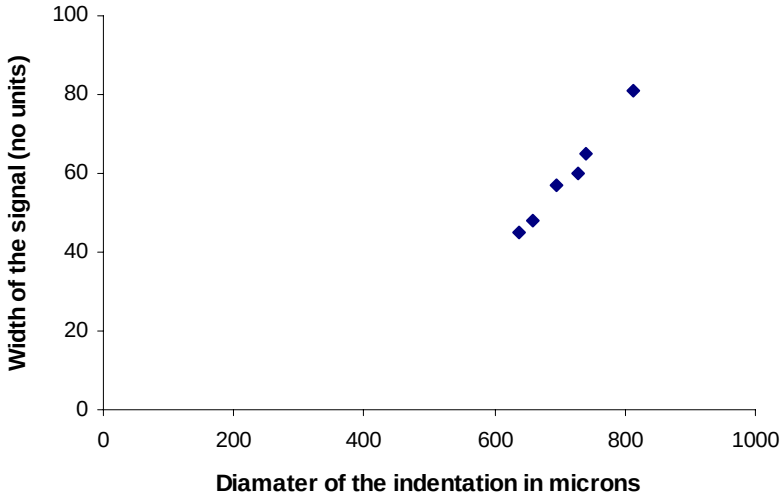

Figure 4-15: Diameter of the indentation vs. width of the signal

It should be noted that for the present fiber optic sensing technique to work, the speed at which the various indentations move beneath the optical fiber should be the same. This

is obvious from the fact that the indentation diameter is correlated with the width of the signal. Unless the speeds are the same for all cases, a correlation cannot be obtained. In the current study, the strength of material has been correlated to the indentation diameter. Thus, the signal received from the optical fiber provides sufficient information to predict the mechanical property of the moving strip.

5. MECHANICAL PROPERTY MEASUREMENT BY LASER SHOCK PROCESSING

The spherical indentation technique is difficult for real time mechanical property measurement of sheet metal in a processing line. Problems arise as the strip is traveling at 2,000 to 4,000 ft/min (10,000 to 20,000 mm/sec) in the processing line. As a first step in developing a process that could be implemented in a real time processing line, the feasibility of using laser shock processing has been investigated. During laser shock processing, an indentation is produced on the metallic target by plastic deformation. The depth of the indentation is an indication of the mechanical property of the material.

5.1 Laser shock processing

When a metallic target is irradiated by an intense (>1GW/cm^2) laser pulse, the surface layer instantaneously vaporizes into a high temperature and high pressure (1-10 GPa) plasma. If the target is covered with a coating, the target is protected from thermal effects and nearly pure mechanical effects are induced. Shock waves are produced by the expanding plasma and mechanical impulses are transferred to the target. The shock pressure causes an indentation on the surface of the metallic target. It should be noted that the indentation is a clear indication of the plastic deformation. It does not involve any thermal effects. This assumption is reasonable because only the coating is vaporized

and the minimum thermal effects are felt by the sample [29]. The schematic representation of LSP is shown in Figure 5-1.

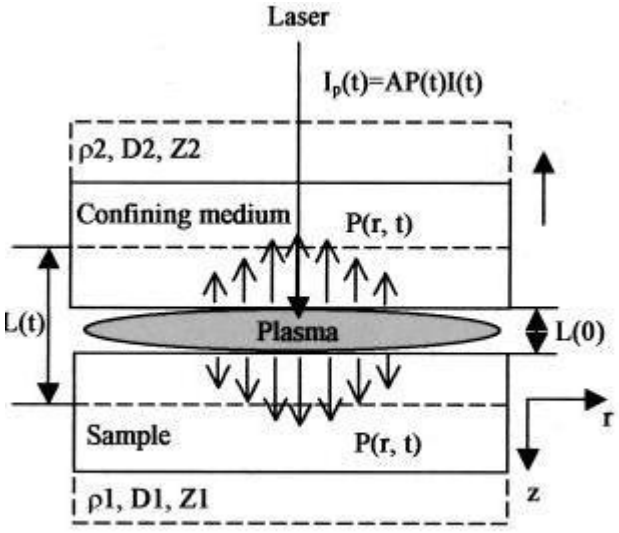

Figure 5-1: Schematic of laser shock processing (LSP) [29]

5.2 Process modeling

Fabbro et al. [9] made a physical study of laser shock processing. He derived the relationship between the shock pressure *P(t)* and the laser intensity *I(t)* as follows:

$$\left(\frac{Z}{2}+\frac{3}{4\alpha}\right)\frac{4}{Z^2}\left(P(t)\right)^2+\left(\frac{3}{Z\alpha}\right)\left(\int P(t)dt\right)\left(\frac{dP(t)}{dt}\right)=I(t) \tag{5.1}$$

Here Z is given as $Z=\dfrac{2}{\left(\dfrac{1}{Z_1}+\dfrac{1}{Z_2}\right)}$ (5-2)

where

Z_1 – impedance of the target material

Z_2 - impedance of the confining medium

α - fraction of internal energy used to increase the thermal energy of the plasma

Thus the pressure developed during the laser shock processing depends upon the incident laser intensity, impedances of the target material and the confining medium and the constant fraction α.

The different temporal laser pulse shapes as outlined by [27] are shown in Figure 5-2.

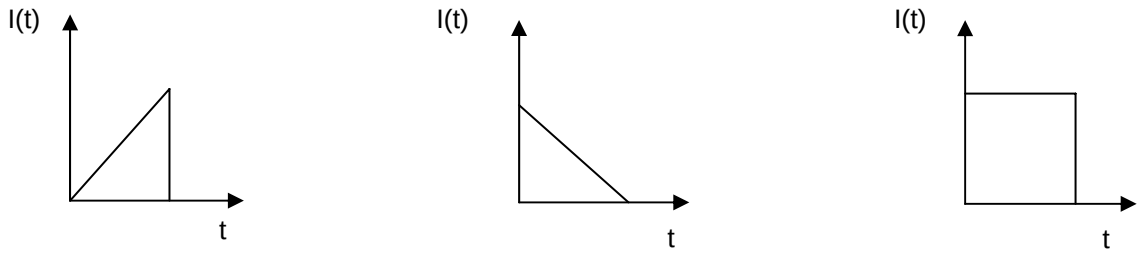

Figure 5-2: Various laser pulse shapes

Zhang et al. [29] used a pulse shape corresponding to Figure 5-3.

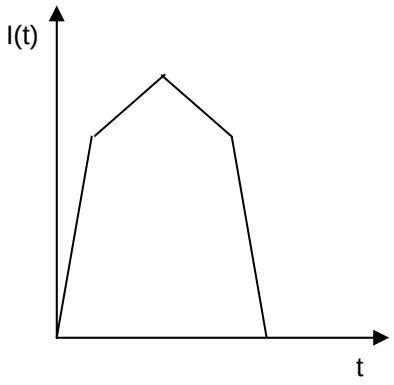

Figure 5-3: Pulse shape used by Zhang et al. [29]

In the current study for simplicity the intensity of the laser beam is assumed to be constant with time throughout the analysis.

$I\ (t)$ = constant = I_0

Assuming a constant laser pulse I_0, Fabbro et al. showed that the pressure developed during the laser pulse is constant with time and is given by

$$P(KBars) = 0.10\left(\frac{\alpha}{1+\alpha}\right)^{0.5} Z^{0.5}(g/cm^2 s) \times I_0{}^{0.5}(GW/cm^2) \qquad (5.3)$$

where I_0 is the intensity of the laser beam.

It is inferred from the above equation that the pressure developed during laser shock processing is directly proportional to the square root of the impedance of the material for the same laser intensity and fraction α. The graph in Figure 5-4 compares the pressure developed for various materials for different laser intensities.

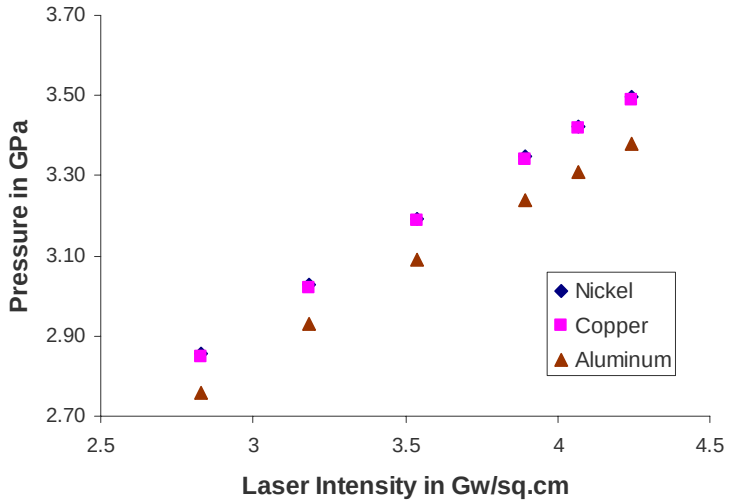

Figure 5-4: Pressure developed for various laser intensities

This pressure is applied for a time period of 50 ns. It should be noted that the duration of the laser pulse must be neither too long nor too short. A long time period causes the target material to evaporate while a short time period does not even cause the coating to evaporate and hence generation of the shock pressure. The pressure existing after the laser pulse has been neglected for simplicity.

The spatial non-uniformity of pressure is considered by assuming a Gaussian distribution. The temporally constant shock pressure P is related to the spatially non-uniform, constant shock pressure P(r) as

$$P(r) = P\exp\left(-\frac{r^2}{2r_o^{\,2}}\right) \tag{5.4}$$

where r is the radial distance from the center of the beam and r_0 is the radius of the laser beam.

5.3 Constitutive equations for material modeling

During laser shock processing the material is subjected to a very high strain rate (of the order of 10^6) and ultra high pressure (2-8 GPa). Hence the constitutive model for material behavior has to include the effect of high strain rate and the ultra high pressure on the material. Johnson et al. [13] studied the effects of the strain rate and temperature on the work hardening behavior of metals. They proposed a model of the form [13]

$$Y = \left(A + B\varepsilon^n\right)\left(1 + C\ln(\frac{\dot{\varepsilon}}{\dot{\varepsilon}_0})\right)K_t \tag{5.5}$$

where A, B and n are material constants

$\dot{\varepsilon}_0$ is the reference strain rates which is usually one

K_t is the constant for including temperature effects

A constitutive model applicable for ultra high pressure was given by Steinberg et al. [34]

$$G = G_0\left[1 + \left(\frac{G'_p}{G_0}\right)P + \left(\frac{G'_T}{G_0}\right)(T - 300)\right] \tag{5.6}$$

$$Y = \sigma_y\left[1 + B(\varepsilon + \varepsilon_0)\right]^n \times \left[1 + \left(\frac{Y'_P}{\sigma_y}\right)P + \left(\frac{G'_T}{G_0}\right)(T - 300)\right] \tag{5.7}$$

where G_0 and σ_y are reference state values of shear modulus and yield strength.

Zhang et al. [29] proposed a model that takes into effect both the pressure and the strain rate by combining the models of Steinberg [24] of Johnson [13].

$$Y = \sigma_y \left[1 + C \ln \dot{\varepsilon} \right] \left[1 + B\varepsilon \right]^n \left[1 + \left(\frac{Y'_P}{\sigma_y} \right) P + \left(\frac{G'_T}{G_0} \right) (T - 300) \right] \tag{5.8}$$

Where C is the logarithmic rate sensitivity at strain rate 1 s^{-1}

B and n are material parameters describing work hardening effect

$\frac{Y_p'}{\sigma_y}$ is the pressure dependence of dynamic yield strength Y

$\frac{G_T'}{G_0}$ is the temperature dependence of the shear modulus G

σ_y is the reference state value of yield strength

G_0 is the reference state value of shear modulus

Reference state corresponds to a temperature of 300 K, pressure of one atmosphere and strain free. The above constitutive equation proposed by Zhang et al. [29] has been used for modeling the material behavior in the current study.

5.4 Finite element modeling of laser shock processing

The deformation of the material in laser shock processing was modeled numerically. Commercial FEM software, ABAQUS, was used to model the LSP process. A cylindrical coordinate system with radial coordinate r, and axial coordinate z was used in all models. A 2-D axi-symmetric model of 200 microns in the r direction and 90 microns in the z direction was developed as shown in Figure 5-5. The bottom surface was

constrained in all directions. The two side faces were traction free while on the top surface the spatially varying pressure was applied. The diameter of the laser beam was 50 microns. The temperature was considered to be 300 K.

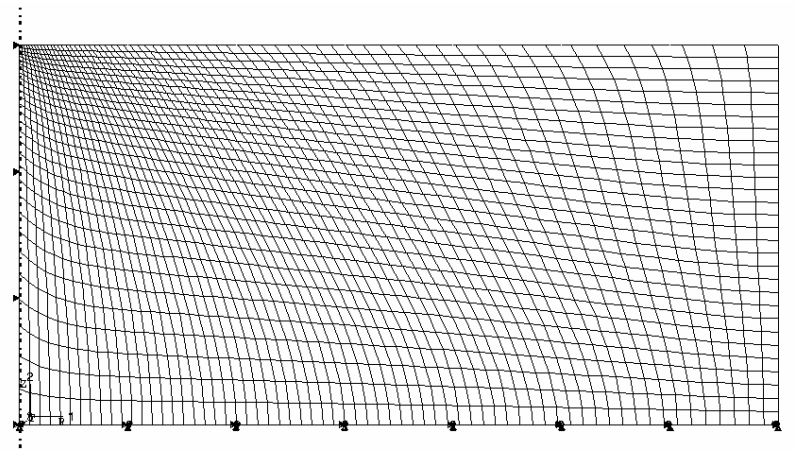

Figure 5-5: Finite element model for laser shock processing

The first step in the simulation was a non-linear dynamic process where the loading was applied for a period of 50 nano-seconds, corresponding to the pulse duration of the Laser beam. In the second step the stresses were allowed to relax for a time period of 1 ms while no load is applied. The constitutive behavior in Equation (5.8) was modeled with the UHARD subroutine while the spatially varying pressure was modeled with the subroutine DLOAD.

UHARD is a user subroutine to define the yield surface size and hardening parameters for isotropic plasticity or combined hardening models [1]. DLOAD is a user subroutine to specify non-uniform distributed loads [1].

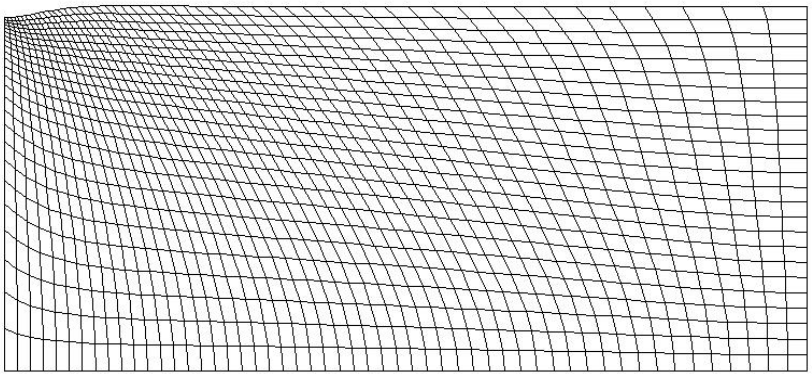

Figure 5-6: Deformed finite element model of laser shock processing

5.4.1 Verification of the developed FEA model

The developed FEA model is compared and validated against the experimental and the model developed by Zhang et al. For verification of the constructed model, the temporal pressure profile was the same as that considered by Zhang et al. [29]. The spatially and temporally varying pressure was then applied to the top face of the axi-symmetric model. Figure 5-6 shows a deformed finite element model subjected to shock pressure. The depth of indentations produced on the target material was used as the criteria for comparison of the model. Single and multiple laser pulses were simulated for copper. Figure 5-7 compares the results between the developed FEA model and the experimental results by Zhang et al. [29] for energy level of 180 μJoules.

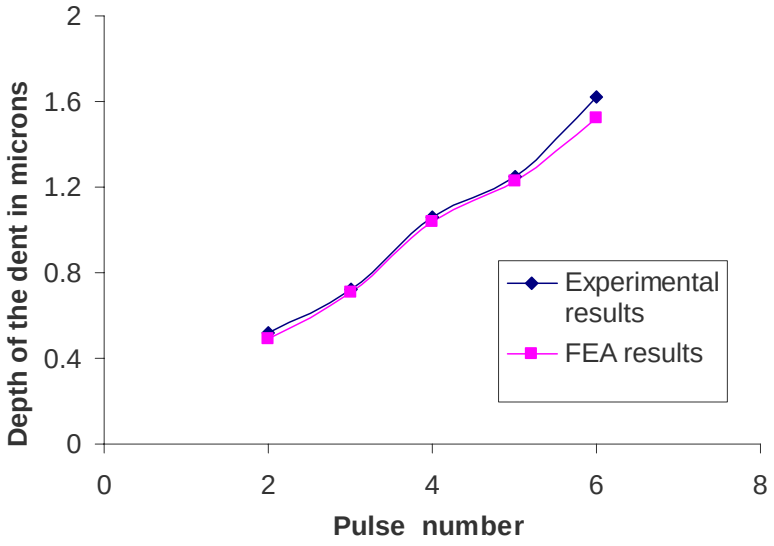

Figure 5-7: Verification of FEA model, E=180 µJoules

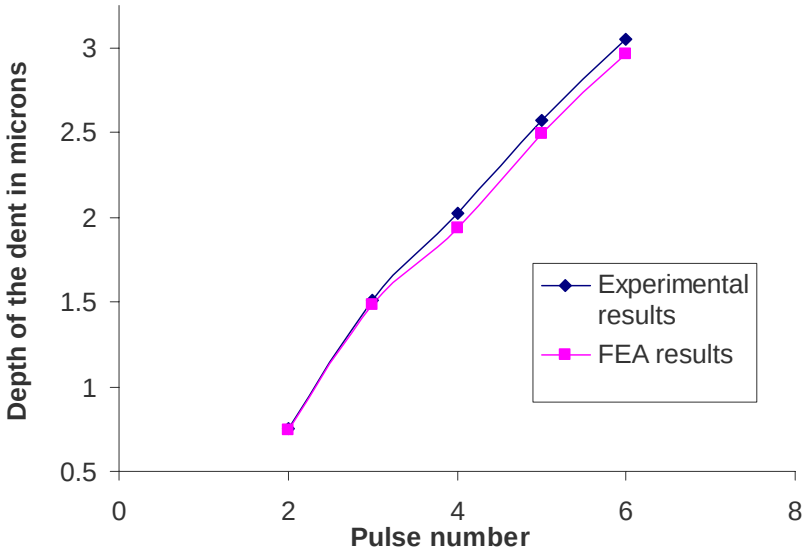

Figure 5-8: Verification of FEA model, E=240 µJoules

Figure 5-8 compares the results between the developed FEA model and the experimental results by Zhang et al. [29] for energy level of 240 μJoules. From the figures, it is seen that the developed FEA code gives results that were in close agreement with the experimental results of Zhang et al. [29]. Thus the predictive capability of the developed FEA model is verified.

5.5 Mechanical property measurement by laser shock processing

Since the indentation produced by laser shock processing is a case of plastic deformation only, not involving melting or vaporization, it is proposed that the depth of the indentation can be used to determine the mechanical properties of the material. Three materials, namely copper, aluminum and nickel were chosen for the study. They were subjected to a single laser pulse of various intensities. Table 5-1 shows the various material properties used in the current study.

Table 5-1: Properties of materials used in the present study

Material	*Reference state Yield strength σ_y (MPa)*	*C*	*B*	*Z (10^7 kg/m^{2}s)*	*n*	*Y_p'/σ_y (TPa^{-1})*
Copper	120	0.027	36	4.18	0.42	28
Aluminum	70	0.01	25	1.5	0.2	65
Nickel	140	0.008	46	4.08	0.53	16

where *C* is the logarithmic rate sensitivity at strain rate 1 s^{-1} .

B and *n* are material parameters describing work hardening effect.

$\frac{Y_p'}{\sigma_y}$ is the pressure dependence of dynamic yield strength *Y*.

σ_y is reference state value of yield strength.

Figure 5-9 compares the depth of the indentation for various laser intensities for the three materials.

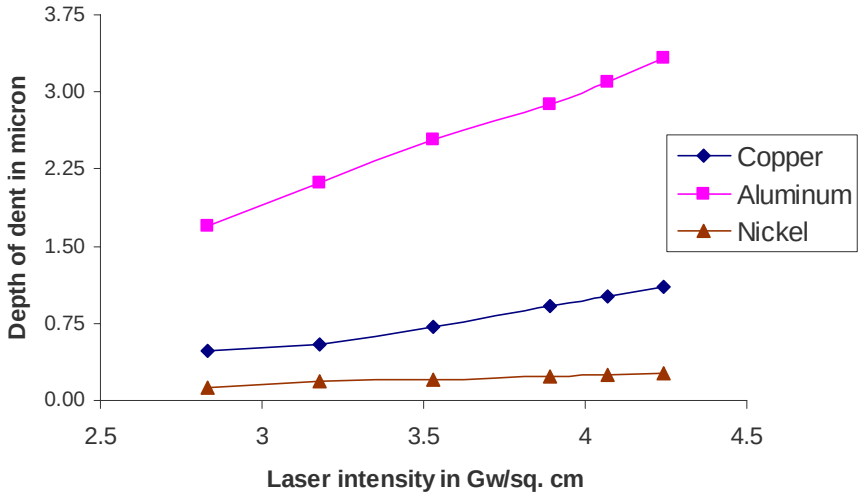

Figure 5-9: Comparison of depth of indentations for different materials

5.5.1 Correlating the mechanical properties of the material

The depth of the indentation is an indication of the strain that has been induced in the material by the shock pressure. Hence, from the constitutive equation, the depth of the indentation h is a function of the yield strength σ_y, material properties C, B, n, Y_p'/σ_y and the pressure P. It should be noted that the laser intensity I_0 and the impedance Z determine the pressure P and hence are automatically considered in the analysis.

$$h = g(\sigma_y, C, B, n, P, \frac{Y_p'}{\sigma_y}) \tag{5.9}$$

The term $\frac{Y_p'}{\sigma_y}$ is a constant and has been determined experimentally for various materials by Steinberg et al. [24]. Here *g* is a function relating the depth of the indentation to the other parameters.

Further investigation is required in the determining the function *g* to calculate the reference state yield strength σ_y and the parameters describing the work hardening effects namely *B* and *n*. Since all the three parameters could vary considerably, they cannot be assumed to be constants. As a part of future work, an analytical model could be developed to determine the mechanical properties mentioned above from the depth of the indentation and the pressure.

6. SUMMARY AND CONCLUSIONS

A new methodology to determine the elasto-plastic properties of a material by spherical indentation technique has been developed. A series of indentations were made on the specimen with a spherical indenter with different loads. The diameter of the indentation was related to the load applied to determine the mechanical properties of the material, namely the yield strength and the work hardening parameters. As seen from the results, the methodology yielded accurate prediction of mechanical properties of the material. However the developed technique tends to become less accurate when the strain hardening exponent *n* is very close to zero. As a part of future work, the combined effect of thickness of the specimen on the depth of the indentation and the anvil effect can be studied.

To facilitate the quick measurement of the diameter of the indentation, a fiber optics sensing technique has been developed. An incident light beam was coupled back into an optical fiber upon reflection from the metal surface. By measuring the diffused light power reflected from the metal surface, the diameter of the indentation was measured. The new technique could measure the diameter of the indentation even at high speeds, which was demonstrated by rotating the specimen. If the fiber optics technique could measure the depth of the indentation along with the diameter of the indentation, then the mechanical properties could be measured from a single indentation.

A preliminary investigation has been conducted to study the feasibility of measuring the mechanical properties of material by laser shock compression. Three materials have been studied for the depth of the indentation at different laser intensities. The parameters affecting the depth of an indentation have been identified. Different laser intensities produce difference depths of the indentation similar to mechanical indentation where different loads produce indentations of different depths. Since the indentation does not involve any thermal effects, the mechanical properties of the material could be predicted from the depth of the indentation. Future work could involve the development of an analytical model to predict the mechanical properties given the laser intensity and the depth of the indentation.

REFERENCES

1. *ABAQUS User's Manual*, version 6.4, Abaqus Inc., 2003.
2. Alcala J., Barone A.C., and Anglada M., "The influence of plastic hardening on surface deformation modes around Vickers and spherical indents," *Acta Metallurgica*, Vol. 48, 2000, pp. 3451-3464.
3. *ASM Metals Reference Book*, American Society for Metals, 1983.
4. Atkins A.G., and Tabor D., "Plastic indentation of metals with cones," *Journal of Mechanics and Physics of Solids*, Vol. 13, 1965, pp. 149-164.
5. Cahoon, J.R., Broughton, W.H., and Kutzak, A.R., "The determination of yield strength from hardness measurements," *Metallurgical Transactions*, Vol. 2, 1971, pp. 1971-1983.
6. Cheng Y.T., and Cheng C.M., "What is indentation hardness?," *Surface and Coatings Technology*, Vol. 133-134, 2000, pp. 417-424.
7. Clauer A.H., and Lahrman D.F., "Laser shock processing as a surface enhancement process," *Key Engineering Materials*, Vol. 197, 2001, 121-144.
8. Clough R.B., Webb S.C., and Armstrong R.W., "Dynamic hardness measurements using a dropped ball with application to 1018 steel," *Materials Science and Engineering*, Vol. A360, 2003, pp. 396-407.
9. Fabbro R., Fournier J., Ballard P., Devaux D., and Virmont J., "Physical study of laser-produced plasma in confined geometry," *Journal of Applied Physics*, Vol. 68, No. 2, 1990, pp. 775-784.

10. Herbert, E.G., Pharr, G.M., Oliver, W.C., Lucas, B.N., and Hay, J.L., "On the measurement of stress-strain curves by spherical indentation," Thin Solid Films, Vol. 398-399, 2001, pp. 331-335.
11. Hill R., Storakers B., and Zdune, "A theoretical study of Brinell hardness test," *Proceedings of the Royal Society of London, series A, Mathematical and Physical Sciences*, Vol. 423, No. 1865, 1989, 301-330.
12. Huber N., Tsagrakis I., and Tsakmakis C., "Determination of constitutive properties of thin metallic films on substrates by spherical indentation using neural networks," *International Journal of Solids and Structures*, Vol. 37, 2000, pp. 6499-6516.
13. Johnson G.R., Hoedfeldt J.M., Lindholm U.S., and Nagy A., "Response of various metals to large torsional strains over a large range of strain rates – Part 1: Ductile metals," *Journal of Engineering Materials and Technology*, Vol. 105, 1983, pp. 42-47.
14. Kucharski S., and Mroz Z., "Identification of hardening parameters of metals from spherical indentation tests," *Journal of Engineering Materials and Technology,* Vol. 123, 2001, pp. 245-250.
15. Kucharski S., and Mroz Z., "Identification of plastic hardening parameters of metals from spherical indentation tests," 2001, *Mat. Sci. Engg*. Vol. A318, pp. 65-76.
16. Ma L., Low S., Song J., and Zhou J., 2003, "Determining mechanical properties of 01 tool steel from reverse computation of indentation measurement," *XVII IMEKO World Congress Metrology in the 3rd Millennium, Croatia*.

17. Nayebi, A., El Abdi, R., and Bartier, O., "New procedure to determine steel mechanical properties from the spherical indentation technique," *Mechanics of Materials*, Vol. 34, 2002, pp. 243-254.
18. Norbury A.L., and Samuel T., "The recovery and sinking-in or piling up of material in the Brinell test, and the relation of these factors on the correlation of the Brinell with certain other hardness tests," *Journal of Iron and Steel Institute,* Vol. 117, 1928, pp. 673-687.
19. Peyre P., Fabbro R., Berthe L., and Dubouchet C., " Laser shock processing of materials, physical process involved and examples of applications," *Journal of Laser Applications*, Vol. 8, 1996, pp. 135-141.
20. Rickerby D.G., "Short communication- Elastic recovery in spherical indentations," *Materials Science and Engineering*, Vol. 56, 1982, pp. 195-196.
21. Robinson W.H., and Truman S.D., "Stress-strain curve for aluminum from a continuous indentation test," *Journal of Materials Science*, Vol. 12, 1977, pp. 1961-1965.
22. Shabel B.S., and Young R.F., "A new procedure for the rapid determination of yield and tensile strength from hardness tests," J.Bussiere (ed.), *Proc.2nd Int. Symp. Nondestructive Characterization of Materials*, Plenum, New York, 1987, pp. 335-343.
23. Shabel B.S., "A simple procedure for calculating Rockwell hardness relationships for metallic alloys," *Material Science and Engineering*, Vol. 95, 1987, pp. 209-216.

24. Steinberg D.J., Cochran S.G., and Guinan M.W., "A constitutive model for metals applicable at high strain rates," *Journal of Applied Physics*, Vol. 51(3), 1980, pp. 1498-1504.
25. Tabor, D., *The Hardness of Metals*, Oxford University Press, London, 1951.
26. Taljat, B., and Zacharia.T., "New analytical procedure to determine stress-strain curve from spherical indentation data," *Int. J. Solids. Structures*, Vol. 35, No.33, 1998, pp. 4411-4426.
27. Thorslund T. and Kar A., "Temperatures, pressures and stresses during laser shock processing," *Optics and Lasers in Engineering*, Vol. 39, 2003, pp. 51-71.
28. Zhang W., and Yao Y.L., "Improvement of laser induced residual stress distributions via shock waves," *ICALEO 2000*, E, 2000, pp. 183-192.
29. Zhang,W. and Yao Y.L., "Micro-scale laser shock processing of metallic components," *Journal of Manufacturing Science and Engineering*, Vol. 124, 2002, pp. 369-378.
30. Zhao F.Z., "Modeling of mechanical behavior of thin films," *Ph.D. thesis, Drexel University,* 1998.

Supplemental Sources Consulted

Asay J.R., and Shahnipoor M., *High-Pressure Shock Compression of Solids*, Springer-Verlag, New York, 1993.

Braisted W., and Brockman R., "Finite element simulation of laser shock peening," *International Journal of Fatigue*, Vol. 21, 1998, pp. 719-724.

Field J.S., and Swain M.V., "Determining the mechanical properties of small volumes of material from sub-micrometer spherical indentation," *Journal of Materials Research*, Vol. 10, No. 1, 1995, pp. 101-102.

Hosford W.F., and Caddell R.M., *Metal Forming, Mechanics and Metallurgy*, Prentice Hall, 1983.

Jayaraman S., Hahn G.T., Oliver W.C., Rubin C.A., and Bastias P.C., " Determination of monotonic stress-strain curve of hard materials from ultra-low-load indentation tests," *International Journal of Solids and Structures*, Vol. 35, No. 5, 1998, pp. 365-381.

Johnson G.R., Hoedfeldt J.M., Lindholm U.S., and Nagy A., "Response of various metals to large torsional strains over a large range of strain rates – Part 2: Less ductile metals," *Journal of Engineering Materials and Technology*, Vol. 105, 1983, pp. 48-53.

Ma D., Xu K., and He J., "A new method of evaluating the yield strength of metal films using depth-sensing indentation experiment," *Acta Metallurgica Sinica*, Vol. 34, No. 6, 1998, pp. 661-666.

Meissner L.P., and Organick I.E., *FORTRAN 77 Featuring Structured Programming*, Addison-Wesley, 1984.

Meyer L.W., "Constitutive equations at high strain rate," *Shock-Wave and High-Strain Rate Phenomenon in Metals*, Marcel Dekker, Inc., 1992, pp. 49-68.

Oliver W.C., and Pharr G.M., “An improved technique for determining hardness and elastic modulus using load and displacement sensing indentation experiments,” *Journal of Material Research*, Vol. 7, No. 6, 1992, pp. 1564-1583.

APPENDIX A

Error reduction algorithm in MATLAB

```
% This program was witten by Bala Janakiraman
% for the error reduction algorithm as a part of the
% thesis of mechanical property measurement
% x is the number of indentations
double a();
x=input('enter the number of indentations');
for i=1:x
   % n is the strain hardening exponents
   n(i)=input('enter the values of n');
end
for i=1:x
   k=0
   nref=n(i)
   for j=1:x
      error=nref-n(j);
      % b is a 2 dimensional matrix that contains all the n's that lies in the vicinity
      % for example all the errors that corresponds to the first
      % value in the data set n(1), will be in the first column of the b
      % matrix
      if error <= 0.05 & error >= -0.05
        % K keeps count of n's which lie in the vicinity of nref
         k=k+1;
         b(j,i)=n(j);
      else
         b(j,i)=0;
      end
   end
```

```
    % a[i] is the array that contains the total number of n's in the
    % vicinity of each n
    a(i)=k;
end
m=1;
total=0;
for i=1:x-1
    if a(i) >= a(m)
        m=i;
    end
end
for i=1:x
    total=total+b(i,m)
end
% nfinal is the final strain hardening exponent
nfinal=total/a(m)
```

APPENDIX B

Input file for finite element analysis of spherical indentation

```
*Heading
 indentation process
** Job name: Job-1 Model name: Model-1
*Preprint, echo=NO, model=NO, history=NO, contact=NO
**
** PARTS
**
*Part, name=Part-2
*End Part
*Part, name=material
*End Part
**
** ASSEMBLY
**
*Assembly, name=Assembly
**
*Instance, name=material-1, part=material
*Node
      1,           0.,           0.
      2,    0.4546912,           0.
      3,    0.9097452,           0.
      4,     1.365885,           0.
      .
      .
   1678,     15.98966,          20.
   1679,     17.23476,          20.
   1680,      18.5694,          20.
   1681,          20.,          20.
*Element, type=CAX4R
   1,    1,    2,   43,   42
   2,    2,    3,   44,   43
   3,    3,    4,   45,   44
   4,    4,    5,   46,   45

1597, 1636, 1637, 1678, 1677
1598, 1637, 1638, 1679, 1678
1599, 1638, 1639, 1680, 1679
1600, 1639, 1640, 1681, 1680
** Region: (Section-1:Picked)
*Elset, elset=_PickedSet2, internal, generate
    1,  1600,     1
** Section: Section-1
*Solid Section, elset=_PickedSet2, material=Mat         erial
1.,
*End Instance
**
*Instance, name=Part-2-1, part=Part-2
```

```
*Node
      1,           0.,     21.24701
      2,           0.,          20.
      3,     3.538149,     21.46708
      4,     3.079512,     21.91515
      .
    408,    0.9097594,     21.51347
    409,    0.6834247,     21.50277
    410,    0.4563103,     21.49802
    411,     0.228511,     21.49636
*Element, type=CAX4R
  1,   1,   8, 104,  43
  2,   8,   9, 105, 104
  3,   9,  10, 106, 105
  4,  10,  11, 107, 106
  .
372, 408, 409,  41,  40
373, 409, 410,  42,  41
374, 410, 411,  43,  42
375, 411, 103,   1,  43
** Region: (Section-2:Picked)
*Elset, elset=_PickedSet2, internal, generate
   1,  375,    1
** Section: Section-2
*Solid Section, elset=_PickedSet2, material=sphere
1.,
*End Instance
*Nset, nset=sphereelementset, instance=Part-2-1, generate
   1,  411,    1
*Elset, elset=sphereelementset, instance=Part-2-1, generate
   1,  375,    1
*Nset, nset=materialelementset, instance=material-1, generate
    1,  1681,     1
*Elset, elset=materialelementset, instance=material-1, generate
    1,  1600,     1
*Nset, nset=bottomelementset, instance=material-1, generate
  1,  41,   1
*Elset, elset=bottomelementset, instance=material-1, generate
  1,  40,   1
*Nset, nset=sideelementset, instance=material-1, generate
    1,  1641,    41
*Elset, elset=sideelementset, instance=material-1, generate
    1,  1561,    40
*Nset, nset=sphereside, instance=Part-2-1
   1,   2,   7,   8,   9,  10,  11,  90,  91,  92,  93,  94,  95,  96,
97,  98
  99, 100, 101, 102, 103
*Elset, elset=sphereside, instance=Part-2-1
   1,   2,   3,   4,   5, 165, 180, 195, 210, 225, 240, 255, 270, 285,
300, 315
 330, 345, 360, 375
*Nset, nset=spheretop, instance=Part-2-1
  5,  6,  7, 58, 59, 60, 61, 76, 77, 78, 79, 80, 81, 82, 83, 84
 85, 86, 87, 88, 89
```

```
*Elset, elset=spheretop, instance=Part-2-1
  90, 105, 120, 135, 150, 151, 152, 153, 154, 155, 156, 157, 158, 159,
160, 161
 162, 163, 164, 165
*Elset, elset=__PickedSurf6_S2, internal, instance=Part-2-1, generate
  5,  75,   5
*Elset, elset=__PickedSurf6_S1, internal, instance=Part-2-1, generate
 76,  90,   1
*Surface, type=ELEMENT, name=_PickedSurf6, internal
__PickedSurf6_S2, S2
__PickedSurf6_S1, S1
*Elset, elset=__PickedSurf7_S3, internal, instance=material-1, generate
 1561,  1600,     1
*Surface, type=ELEMENT, name=_PickedSurf7, internal
__PickedSurf7_S3, S3
*Elset, elset=_bottomsurfacemat_S1, internal, instance=material-1,
generate
  1,  40,   1
*Surface, type=ELEMENT, name=bottomsurfacemat
_bottomsurfacemat_S1, S1
*Elset, elset=_sidesurfacemat_S4, internal, instance=material-1,
generate
    1,  1561,    40
*Surface, type=ELEMENT, name=sidesurfacemat
_sidesurfacemat_S4, S4
*Elset, elset=_sphereside_S2, internal, instance=Part-2-1, generate
 165,  375,   15
*Elset, elset=_sphereside_S1, internal, instance=Part-2-1, generate
 1,  5,  1
*Surface, type=ELEMENT, name=sphereside
_sphereside_S2, S2
_sphereside_S1, S1
*Elset, elset=_spheretop_S2, internal, instance=Part-2-1, generate
  90,  150,   15
*Elset, elset=_spheretop_S1, internal, instance=Part-2-1, generate
 151,  165,    1
*Surface, type=ELEMENT, name=spheretop
_spheretop_S2, S2
_spheretop_S1, S1
*End Assembly
**
** MATERIALS
**
*Material, name=Material
*Density
8000.,
*Elastic
 7e+10, 0.3
*Plastic
  6.7e+07,   0.
  7.7e+07, 0.04
  8.5e+07, 0.08
  9.8e+07, 0.12
 1.05e+08, 0.16
```

```
*Material, name=sphere
*Density
9000.,
*Elastic
 7e+12, 0.3
**
** INTERACTION PROPERTIES
**
*Surface Interaction, name=IntProp-1
*Friction
0.,
*Surface Behavior, pressure-overclosure=HARD
** ----------------------------------------------------------------
**
** STEP: Step-1
**
*Step, name=Step-1
Explicit step for the indentation process
*Dynamic, Explicit
, 0.05
*Bulk Viscosity
0.06, 1.2
**
** BOUNDARY CONDITIONS
**
** Name: bottommat Type: Displacement/Rotation
*Boundary
bottomelementset, 1, 1
bottomelementset, 2, 2
bottomelementset, 6, 6
** Name: sidesonstraint Type: Displacement/Rotation
*Boundary
sideelementset, 1, 1
** Name: sidesphere Type: Displacement/Rotation
*Boundary
sphereside, 1, 1
**
** LOADS
**
** Name: Load-1   Type: Pressure
*Dsload
spheretop, P, 8e+07
**
** INTERACTIONS
**
** Interaction: Int-1
*Contact Pair, interaction=IntProp-1, mechanical constraint=KINEMATIC,
cpset=Int-1
_PickedSurf7, _PickedSurf6
**
** OUTPUT REQUESTS
**
*Restart, write, number interval=1, time marks=NO
**
```

```
** FIELD OUTPUT: F-Output-1
**
*Output, field, variable=PRESELECT
**
** HISTORY OUTPUT: H-Output-1
**
*Output, history, variable=PRESELECT
*End Step
```

APPENDIX C

Input file for the finite element of laser shock processing

```
*Heading
 Finite element of laser shock processing
** Job name: Job-1 Model name: Model-1
*Preprint, echo=NO, model=NO, history=NO, contact=NO
**
** PARTS
**
*Part, name=Copper
*End Part
**
** ASSEMBLY
**
*Assembly, name=Assembly
**
*Instance, name=Copper-1, part=Copper
*Node
      1,           0.,           0.
      2,        4e-06,           0.
      3,        8e-06,           0.
      4,      1.2e-05,           0.
      .
      .
   2343,     0.000188,        9e-05
   2344,     0.000192,        9e-05
   2345,     0.000196,        9e-05
   2346,       0.0002,        9e-05
*Element, type=CAX4R
   1,    1,    2,   53,   52
   2,    2,    3,   54,   53
   3,    3,    4,   55,   54
   4,    4,    5,   56,   55
   .
   .
2247, 2291, 2292, 2343, 2342
2248, 2292, 2293, 2344, 2343
2249, 2293, 2294, 2345, 2344
2250, 2294, 2295, 2346, 2345
** Region: (Section-1:Picked), (Controls:EC-1)
*Elset, elset=_PickedSet2, internal, generate
    1,  2250,     1
** Section: Section-1
*Solid Section, elset=_PickedSet2, controls=EC-1, material=Material-1
1.,
*End Instance
*Nset, nset=_PickedSet15, internal, instance=Copper-1, generate
  1,  51,   1
*Elset, elset=_PickedSet15, internal, instance=Copper-1, generate
  1,  50,   1
```

```
*Elset, elset=__PickedSurf16_S3, internal, instance=Copper-1, generate
 2201,  2250,     1
*Surface, type=ELEMENT, name=_PickedSurf16, internal
__PickedSurf16_S3, S3
*End Assembly
**
** ELEMENT CONTROLS
**
*Section Controls, name=EC-1, hourglass=RELAX STIFFNESS
1., 1., 1.
**
** MATERIALS
**
*Material, name=Material-1
*Density
8960.,
*Elastic
 1.2e+11, 0.3
*Plastic, hardening=USER, properties=5
 1.2e+08,  0.45,   36., 0.027, 1e-11
** ----------------------------------------------------------------
**
** STEP: Step-1
**
*Step, name=Step-1, nlgeom=YES, amplitude=RAMP, inc=10000
Variation of load
*Dynamic,alpha=-0.333,haftol=25.
5e-09,70e-09,2e-15,70e-09
*Solution Technique, Type=Quasi-Newton
*Controls,Analysis=Discontinuous
*Controls,Parameters=Time Incrementation
,,,,,,,9,6,10
**
** BOUNDARY CONDITIONS
**
** Name: BC-1 Type: Displacement/Rotation
*Boundary
_PickedSet15, 1, 1
_PickedSet15, 2, 2
_PickedSet15, 6, 6
**
** LOADS
**
** Name: Load-1   Type: Pressure
*Dsload
_PickedSurf16, PNU, 1e-06
**
** OUTPUT REQUESTS
**
*Restart, write, frequency=1
**
** FIELD OUTPUT: F-Output-1
**
*Output, field, variable=PRESELECT
```

```
**
** HISTORY OUTPUT: H-Output-1
**
*Output, history, variable=PRESELECT
*El Print, freq=999999
*Node Print, freq=999999
*End Step
```

Subroutines UHARD and DLOAD

```
C
      SUBROUTINE UHARD(SYIELD,HARD,EQPLAS,EQPLASRT,TIME,DTIME,TEMP,
     $     DTEMP,NOEL,NPT,LAYER,KSPT,KSTEP,KINC,
     $     CMNAME,NSTATV,STATEV,NUMFIELDV,
     $     PREDEF,DPRED,NUMPROPS,PROPS)
C
      INCLUDE 'ABA_PARAM.INC'
C
      CHARACTER*80 CMNAME
C
      DIMENSION HARD(3),STATEV(NSTATV),TIME(*),
     $          PREDEF(NUMFIELDV),DPRED(*),PROPS(*)
C
      YSTRESS=SYIELD
      PRINT *,YSTRESS,TIME(1)
      XSIG=PROPS(1)
      XTIME=TIME(1)
      XN=PROPS(2)
      XC=PROPS(4)
      XB=PROPS(3)
      XYDASH=PROPS(5)
      XSRATE=EQPLASRT
      XPRESS=1.2e09
      XTIME=TIME(1)
      A1=25E-09
      B1=50E-09
C   ************************************
      XEQPLAS = EQPLAS
      T2=(1+XB*XEQPLAS)**XN
      T3=(1+XYDASH*XPRESS)
C   ************************************
      IF (XSRATE .LE. 1.0) THEN
         XSYIELD=XSIG*T2
      END IF
C   ************************************
      IF (XSRATE .GT. 1.0)  THEN
      T1=1+XC*LOG(XSRATE)
      XSYIELD=XSIG*T1*T2
      END IF
C   ************************************
      IF(YSTRESS .EQ. 0.0) THEN
      YSTRESS=1.2E08
      END IF
```

```
C   ************************************
      IF(XSYIELD .GT. YSTRESS) THEN
      SYIELD = XSYIELD
      END IF
C   * ************************************
      IF(XSYIELD .LE.YSTRESS) THEN
      SYIELD=YSTRESS
      END IF
C   ************************************
C      SYIELD=XSYIELD
C      PRINT *,XSYIELD,XSRATE
      RETURN
      END
C
       SUBROUTINE DLOAD(F,KSTEP,KINC,TIME,NOEL,NPT,LAYER,KSPT,COORDS,
     1                 JLTYP,SNAME)
      INCLUDE 'ABA_PARAM.INC'
      DIMENSION COORDS(3),TIME(2)
      CHARACTER*80 SNAME
C     print *,COORDS(1)
      XRADIUS=COORDS(1)
      TR = 25e-6
      XTIME=TIME(1)
      XPRESS=1.2e09
      C   ****************************************************
      F=XPRESS*exp(-(XRADIUS*XRADIUS)/(2*TR*TR))
C      print *,XPRESS,XTIME
      RETURN
      END
```

VITA

Balasubramanian Janakiraman

44, Dhanalakshmi Colony, First Street

Vadapalani, Chennai – 600026, India.

March 11, 1981 ……..Born, Chennai, India

2002 – 2004……...….M.S. Mechanical Engineering

Texas A&M University, USA

1998 – 2002……..B.E. Mechanical Engineering

Madurai Kamaraj University, India

Email Address: balasub18@yahoo.com